ABSTRACT

LEE, KYOUNG OOK. Particle Tracking Using Molecular Dynamics Simulation For Pebble Bed Reactors. (Under the direction of Robin P. Gardner.)

Characteristics of the pebble tracks generated through Molecular Dynamics (MD) Simulations were investigated for a Pebble Bed Reactor (PBR). Through monitoring the mass flow rate and its resultant local volume fraction as well as the local coordination numbers (the local means that were defined by the regime within the separate parts of the reactor; the coordination number is defined as the number of contacting its neighbors), the pebble piling up and subsequent discharge were investigated. Simulations were then conducted through the implementation of the non-cohesive Hertz-Mindlin theory. The governing equation can be derived from Lagrangian dynamics that are given by the kinetic and potential energies. The kinetic energy consists of the translational and the rotational kinetic energies and the potential energy consists of the gravitational and the Hertz potentials. MD simulation builds off of the virial theorem (relating to the system of forces and their positions) which states that the stress energy tensor is in relation to the gravitational potential and the Hertz potential. The output of the simulation data gives the force, the velocity, and the position of the particles. Calculation from the interactions between the particles resides within the Hertz-Mindlin potential. These interactions resulted in a pilling effect from the deposited particles being simply dropped into the hopper of the PBR. At which point, the discharge in the local region was observed and from this it was then determined if the jamming phenomenon was occurring. The phase diagram of the volume fraction and the coordination number was found to yield the transition of the jamming or flowing condition. Regardless of the situation experienced, the mass flow rate and the phase diagram agreed on the flow established. Specific analysis

المنارة للاستشارات

www.manaraa.com

on the flowing condition requires a heterogeneous medium that can influence the wall applied shear and normal stresses which are then used to determine the pebble flow and to evaluate their subsequent energies. When implementing the MD simulation, it was found that a random walk process within Monte Carlo simulation was the most accurate approach to the solution.

المنارة للاستشارات
www.manaraa.com

© Copyright 2011 by Kyoung Ook Lee

All Rights Reserved

المنارة للاستشارات

www.manaraa.com

Particle Tracking Using Molecular Dynamics Simulation For Pebble Bed Reactors

by
Kyoung Ook Lee

A dissertation submitted to the Graduate Faculty of
North Carolina State University
in partial fulfillment of the
requirements for the Degree of
Doctor of Philosophy

Nuclear Engineering

Raleigh, North Carolina

2011

APPROVED BY:

Yousry Y. Azmy	Dmitriy Y. Anistratov
J. David Brown	Robin P. Gardner Chair of Advisory Committee

المنارة للاستشارات
www.manaraa.com

DEDICATION

I dedicate this thesis to my father, the late Dae Hyun Lee, who passed away in May of 2005, my mother Sook Hee Lee, also my brother and sister. I also dedicate this to my wife, Young Hee Kim, and my loving sons, Julian and Robin.

المنارة للاستشارات
www.manaraa.com

BIOGRAPHY

Kyoung O. Lee was born in Seoul, South Korea, on May 21, 1975. He was admitted to the graduate program at North Carolina State University in August 2005 in the Department of Nuclear Engineering. Since 2005, he has been working towards his doctoral degree through working for the Center for Engineering Applications of Radioisotopes (CEAR) of Nuclear Engineering at North Carolina State University (NCSU) under the guidance of Dr. Robin P. Gardner. While at NCSU, he obtained his double Master of Science degree in Physics 2010 and Nuclear Engineering 2007.

www.manaraa.com

ACKNOWLEDGEMENTS

I am deeply indebted to all those that have supported me for providing encouragement and contributions for this endeavor during my degree.

First of all, I would like to express my deep gratitude to Dr. Robin P. Gardner for granting me his support and valuable advice during my research and education. He has shown enthusiasm and inspired me to work in academics and is a role model for my future carrier. Special gratitude is extended to Dr. Yousry Y. Azmy, my committee for the Department of Nuclear Engineering for supporting my research and graduate studies. I would also like to thank my committee members, Dr. Dmitriy Y. Anistratov, and Dr. J. David Brown for their trust and discussions. This work was supported by the Nuclear Energy Research Initiative (NERI) Program of the US Department of Energy. I wish to express my special appreciation to Adan Calderón for assistance during my research. I would also like to thank my colleagues, Wesley Holmes, Richard Howard, Cody Peeples, and Johanna Peeples. Special thanks are given to my friends, Eui-Seok Kim in South Korea, Uk Huh in Tennessee, and Ucheor Brandon Choi in New York. I also wish to express my appreciation to my friends, Guk-ho Gil, and Jaewook Seok at NCSU. Special gratitude is also extended to Dr. Man-Sung Yim, Dr Chueng R. Ji and Dr. Chang B. Kim. I am deeply grateful to them for their encouragement and a careful guidance during my graduate studies.

Finally, I would like to thank my family, who has always supported me and given me their endless guidance or love during my education.

www.manaraa.com

TABLE OF CONTENTS

المنارة للاستشارات

www.manaraa.com

المنارة للاستشارات

www.manaraa.com

LIST OF TABLES

المنارة للاستشارات
www.manaraa.com

LIST OF FIGURES

www.manaraa.com

www.manaraa.com

للاستشارات المنارة

www.manaraa.com

Chapter 1

Introduction

In recent years, Molecular Dynamics (MD) Simulations or the Discrete Element Method (DEM), introduced by Cundall and Strack (1979) has been recognized as a crucial numerical tool to simulate granular dynamics in Pebble Bed Reactors (PBRs) in order to broaden our understanding of complex phenomena. These simulations are improved models that closely resemble physical reality and validate the experimental process leading to optimum scientific progress. For Pebble Bed Reactors, the Hertz-Mindlin contact theory (Johnson 1985) was used by Rycroft, Grest et al. (2006). The contact parameters turned out to have a significant influence in previous work, Brilliantov, Spahn et al. (1996); Silbert, Ertas et al. (2001), Zhang and Makse (2005). PBRs were performed by Gan, Kamlah et al.(2010); Li,Yong et al. (2009). The simulation results were in good agreement with the experiment. Successively, our approach uses an noncohesive and deformable contact dynamics through the stress and strain relation results in a more accurate method. For MD simulation and field estimates, the computational code LAMMPS/LIGGGHTS has been used because of its efficient algorithm. Wall stress field is implemented by the LIGGGHTS code for granular flow with the MD simulation. The

المنارة للاستشارات
www.manaraa.com

Hertz-Mindlin theory begins with the static pattern forming interface for the dynamic pattern coupled to the MD simulation. When pebbles are transported down in the cylindrical vessel to the regions inside the hopper created by a conical angle determined by geometrical conditions, the type of flow and the flow rate will have important roles in PBRs that indicate the like-solid or like-fluid phase transition, Jaeger, Nagel et al. (1996); Ono, O'Hern et al. (2002). This data analysis can be investigated by a velocity profile, streamline for particle tracking, and random packing fraction etc. The simulation results were compared and then validated by statistical modeling. A natural way to describe granular motion is through the continuum approach, where the grains are not thought to be composed of discrete particles, but rather are treated as continuously filling the regions.

1.1 Literature Review

This review mainly refers to a systematic representation of recent papers, which described the theoretical view of particle tracking method in Pebble Bed Reactors (PBRs). We summarize the recent results of various models consistent with experimental results in PBRs. A general theory of granular flow does not exist although many efforts have been made to complete a universal equation to predict the behavior of granular media, which is recognized to deal with occasionally fluid-like, solid-like or gas-like behavior (Jaeger, Nagel et al. 1996). A granular material consists of a number of discrete solid particles and an interstitial space. Granular dynamics is very complex due to many body interactions. Particularly in PBRs, the obstacle of a bulk particles arching or locking in a conical hopper or silo might occur to drain out these materials or decrease flow

المنارة للاستشارات
www.manaraa.com

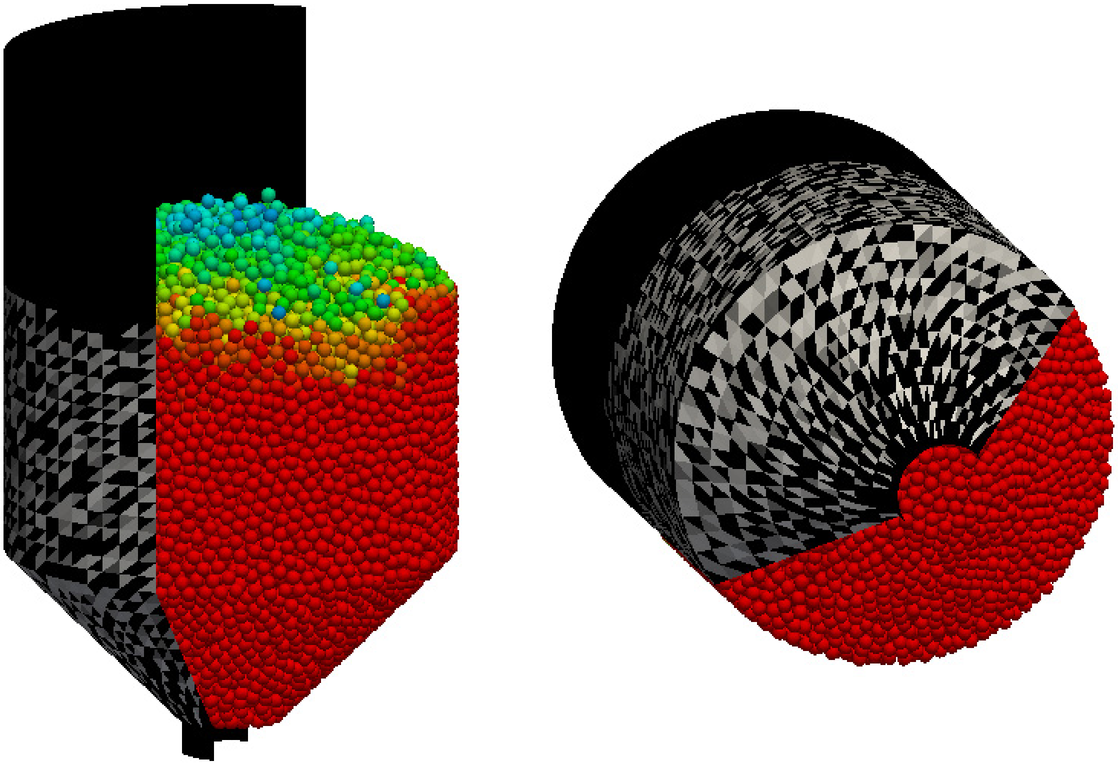

Figure 1.1: Configuration for Pebble Bed Reactor design of the conical hopper and pebble locations with wall stress from two different points of view (side and bottom) by MD simulation

www.manaraa.com

velocity. The macroscopic motions in gravity-driven systems are governed by not only the geometry and external boundary condition of the silo but also flow properties of granular materials, such as friction, viscosity and porosity. Obviously, an understanding of the pebbles transportation is very important to generate the reactor. The probability of pebble transition is regarded as a random walk imposed according to a velocity scale. By determining the velocity distribution, our main aim is to gain insight into how the velocity distribution of pebbles is essentially adapted when statistical state prevails. We show how this theoretical approach can be extended to acquire the significant parameters involved.

1.1.1 Monte Carlo PBR Pebble Tracking Simulation Via a Random Walk Approach

Using Monte Carlo (MC) simulation, random walks are used for pebble (particle) tracking in a two-dimensional geometry in the presence of a biased gravity field. The MC simulation is developed with free-grid transport of a particle with random effects for implementing the convection diffusion equation. Investigation of the effect of viscosity damping in the presence of Gaussian random fluctuation superimposed on an external force is considered. A macroscopic description of granular flow patterns can be accomplished with a Stochastic Method in the discrete medium of a pebble (particle) packing structure using the effect of random fluctuations, Caram and Hong (1991). The motion of particles can be described for many different aspects of the flow. It is often used for MC simulation for granular flow trajectories, which is closer to the benchmark of a radioactive tracer method for the development of mathematical models, Gardner, Barrett et al.

المنارة للاستشارات
www.manaraa.com

(1996). This fluid-like behavior is collectively characterized by the Langevin equation for describing Brownian particle movement by changing directions in particle collisions. The MC simulation implements the use of random walks in two-dimensional or three-dimensional convection diffusion equations. This method uses free-grid transport of a particle, which carries the effect of viscosity damping by Gaussian random fluctuation in the presence of an external force.

Convection diffusion equation

The convection diffusion equation in two dimensions can mathematically be described by the concentration $C(r, t)$ of diffusing particles using Fick's Law

$$J = -K\frac{\partial C\left(r,t\right)}{\partial x} - K\frac{\partial C\left(r,t\right)}{\partial z} + \left\langle u\right\rangle C\left(r,t\right) \tag{1.1}$$

and the continuity equation

$$\frac{\partial C\left(r,t\right)}{\partial t} + \nabla \cdot J = 0 \tag{1.2}$$

The convection-diffusion equation has the solution

$$\frac{\partial C\left(r,t\right)}{\partial t} = K\frac{\partial^2 C\left(r,t\right)}{\partial x^2} + K\frac{\partial^2 C\left(r,t\right)}{\partial z^2} - \left\langle u\right\rangle \frac{\partial C\left(z,t\right)}{\partial z} \tag{1.3}$$

where K is the virtual coefficient of diffusion (m^2/s) and $\langle u\rangle$ is the mean velocity of the center of mass arising from the external force on the particles. Without a convection term, the interpretative solution is the mean distance, $\langle \Delta r\left(t\right)\rangle = 0$, and the mean square distance, $\langle \Delta r^2\left(t\right)\rangle = 4Dt$, where the boundary condition $C\left(\pm\infty, t\right) = 0$.

www.manaraa.com

The Langevin Equation

The spatial direction random walk carriers has two parameters, a granular particle and the biased random walk placed in an external force field pulled downward by the gravitational force. Two-dimensional random walks have been updated every time automatically, where a trial position has been defined by pseudo-random numbers in real interval (0,1) with uniform distribution. The direction was then given in four different walks accompanied by random vertical and horizontal shifts, with the probability of $\xi_i = 1/4$ $(i = 1, 2, 3, 4)$ where this sum should be $\sum \xi_i = 1$.

The Langevin equation then becomes

$$m\frac{d\mathbf{v}}{dt} = mg - \gamma\mathbf{v} + \mathcal{F}(t) \tag{1.4}$$

where in a viscous medium, the frictional coefficient γ is slowing it down, and a random fluctuation-dissipation term, denoted by $\mathcal{F}(t)$, is a Gaussian distribution of random variables with zero mean and the variance varies in an irregular fashion of time t.

According to the x, z transformation by the Langevin equation when the velocity is at steady state, $\frac{d\mathbf{v}}{dt} = 0$

- x direction

$$x\left(t + \delta t\right) = x\left(\delta t\right) + v_x \delta t \tag{1.5}$$

$$v_x\left(\delta t\right) = -m/\gamma\mathcal{F}(t)$$

www.manaraa.com

- z direction

$$z\left(t+\delta t\right)=z\left(\delta t\right)+v_z\delta t \tag{1.6}$$
$$v_z\left(\delta t\right)=-m/\gamma g+m/\gamma\mathcal{F}(t)/m$$

where $\delta t=t_{n+1}-t_n$ (n, the number of discrete time steps).

In the second phase, the MC algorithm can be derived that it combines with the diffusive term.

$$\mathcal{F}(t)=\sqrt{2D\delta t}p\left(t\right) \tag{1.7}$$

In this case the Monte-Carlo method using the Gaussian probability density function (PDF) has the form $p\left(\varphi\right) = \frac{1}{\sqrt{2\pi}}\exp\left(-\frac{\varphi^2}{2}\right)$, denoted by φ, an arbitrary number to normally distributed random numbers with zero mean and unit standard deviation. The Gaussian random variable is equivalent to $\mathcal{F}(t)$ that is represented by the motion in the opposite direction.

Thus simplifying and arranging as

$$x\left(t+\delta t\right)=x\left(\delta t\right)\pm m/\gamma\mathcal{F}(t)\delta t \tag{1.8}$$
$$z\left(t+\delta t\right)=z\left(\delta t\right)-m/\gamma g\pm m/\gamma\mathcal{F}(t)\delta t$$

If many trials are used, the mean square distance can be evaluated to $\langle\Delta r^2\left(t\right)\rangle = \langle\Delta x^2\left(t\right)\rangle+\langle\Delta z^2\left(t\right)\rangle$.

The particle tracking in Figures 1.2 and 1.3 show that the particles have erratic paths due to a biasing term. There is a critical need for better methods of analysis in order

www.manaraa.com

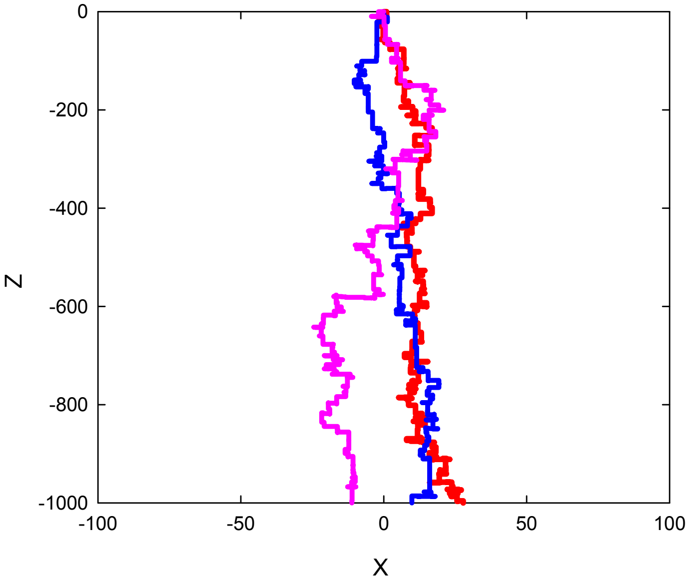

Figure 1.2: Single particle tracking trajectory in two dimensional motion by placing an initial condition on the vertical and horizontal positions, z=0 and x=0 with three trial runs

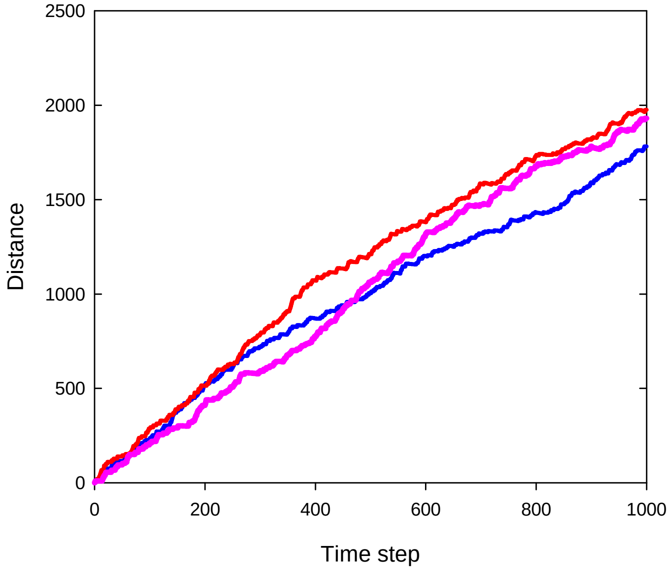

Figure 1.3: Travel distance by placing an initial condition on the height, z=0 and x=0 with the identical samples (color) on the corresponding Fig. 1.1

www.manaraa.com

to understand the fine spatial scale and the density aspects of the granular dynamics in PBRs. The MC approach presented here appears to be such a method using the New Kinematic Model (Chapter 2) and the Monte Carlo Simulation describes a benchmark that implemented a radioisotope tracer method, for granular flow that explicitly accounts for changes in the density field, Gardner, Barrett et al. (1996). In addition to statistical analysis, random walks of the time step are related with the probability function on a formal description of convection-diffusion. The Langevin equation can be shown to obey the Einstein relation of effective temperature for the diffusion coefficients. To understand a granular model due to a critical bulk density, it is necessary to use the density transition of the model known as the approach of Edwards (Mehta and Edwards 1989). The nonequilibrium phase transition can be characterized by the probability distribution by extending the packing fraction for granular fluids with elastic or inelastic collisions.

1.1.2 Granular Dynamics using Langevin and Fokker Planck Equation

Langevin equation with friction is applied under the influence of the gravitational field. We also discuss the relation with Fokker-Planck Equation using detailed balance and Metropolis-Hastings algorithm. The collisional entropy can explain a granular jamming phenomenon. In recent years, there has been considerable interest in understanding the dynamics of granular particles which is crucial to many applications. The diffusion has been found to be influenced by the local thermal equilibrium. In this work, a collisional term involves the Langevin equation and the Fokker-Planck equation describing each interaction of the granular particles. One probability of the Detailed balance

المنارة للاستشارات
www.manaraa.com

and Metropolis-Hastings algorithm for a Markov Chain Monte Carlo methods is a non-Maxwellian distribution function with the mean velocity of the field particles and a effective temperature. Another probability explains the entropy in collisional term towards jamming phenomenon.

The macroscopic behavior of a particle with a granular mass m that is placed in an external force field which pulls downward due to the gravitational force is examined. The Langevin equation (Reif, F. (1965) and Huang, K. (1987)) then becomes

$$m\frac{d\mathbf{v}}{dt} = mg - \gamma\mathbf{v} + \mathcal{F}(t) \tag{1.9}$$

where the frictional coefficient is γ, and a random fluctuation-dissipation term denoted by $\mathcal{F}(t)$ which very little is known abut because it varies in an irregular fashion with respect to time t. We assumed the mean value with $\langle\mathcal{F}(t)\rangle = 0$ and the correlation with $\langle\mathcal{F}(t)\mathcal{F}(t')\rangle = \zeta\delta(t-t')$

Taking the mean value of both sides and considering the steady state situation, $d\langle v\rangle/dt = 0$, Thus one obtains

$$mg - \gamma\langle\mathbf{v}\rangle = 0 \tag{1.10}$$

This shows that $\langle\mathbf{v}\rangle = \frac{m}{\gamma}g$. The relation is then given by Einstein relation as $D = kT/\gamma$, from the Langevin equation where the temperature relation with the diffusion coefficient D and a fictional coefficient γ by its particle-surface.

Given the Langevin equation associated with an expression for the Fokker-Planck $f(r,\mathbf{v},t)$, a derivation of the general equation of the Fokker-Planck relation which includes collisions and represents the particles driven by gravity is presented. The Fokker-Planck equation that includes the collisional term is

www.manaraa.com

$$
\begin{aligned}
&\frac{\partial f}{\partial t} + \mathbf{v} \cdot \nabla_r f + \left(g - \frac{\gamma}{m}\mathbf{v}\right) \cdot \nabla_v f \\
&= \int \left(f(\mathbf{v}_i)f(\mathbf{v}_j) - f(\mathbf{v}'_i)f(\mathbf{v}'_j)\right) \sigma(\mathbf{v}_i, \mathbf{v}_j \rightarrow \mathbf{v}'_i, \mathbf{v}'_j) d\Omega' d^3\mathbf{v}_i d^3\mathbf{v}_j d^3\mathbf{v}'_i
\end{aligned}
\tag{1.11}
$$

Constraining the scattering probabilities when $(\mathbf{v}_i, \mathbf{v}_j) \rightarrow \left(\mathbf{v}'_i, \mathbf{v}'_j\right)$, each particle with the differential scattering cross-section has the interaction between them. In particular, this occurs within the so-called inverse collision by interchanging the particles of initial and final states. The original and inverse collisions are identical to the Fokker-Planck equation

$$
\sigma(\mathbf{v}_i, \mathbf{v}_j \rightarrow \mathbf{v}'_i, \mathbf{v}'_j) = \sigma(\mathbf{v}'_i, \mathbf{v}'_j \rightarrow \mathbf{v}_i, \mathbf{v}_j) \tag{1.12}
$$

The cross-section, $\sigma(\mathbf{v}_i, \mathbf{v}_j \rightarrow \mathbf{v}'_i, \mathbf{v}'_j) \approx W(\mathbf{v}|\mathbf{v}')P(\mathbf{v}, t)$ can be found from the Markov chain Monte Carlo methods. Many interaction distributions of a stochastic velocity $\mathbf{v}$ involve a local thermodynamic equilibrium in the diffusion coefficient as given by the Einstein relation. This allows us to consider $P(\mathbf{v}, t) = P(\mathbf{v})$ for enough time. When the condition of detailed balance is satisfied, we have

$$
\sigma(\mathbf{v}_i, \mathbf{v}_j \rightarrow \mathbf{v}'_i, \mathbf{v}'_j) = W(\mathbf{v}|\mathbf{v}')P(\mathbf{v}) \tag{1.13}
$$

where $W(\mathbf{v}|\mathbf{v}')$ is the cross-section probability of the system which changes from a state $\mathbf{v} \rightarrow \mathbf{v}'$. For a system in thermodynamic equilibrium between the state rate $W(\mathbf{v}|\mathbf{v}')$ and the reverse $W(\mathbf{v}'|\mathbf{v})$, the detailed balance and Metropolis-Hastings algorithm finds that

www.manaraa.com

$$W(\mathbf{v}|\mathbf{v}')P(\mathbf{v}) = W(\mathbf{v}'|\mathbf{v})P(\mathbf{v}') \tag{1.14}$$

Under the detailed balance and Metropolis-Hastings algorithm, the probability ratio imposes the condition of detailed balance as

$$\frac{W(\mathbf{v}|\mathbf{v}')}{W(\mathbf{v}'|\mathbf{v})} = \frac{P(\mathbf{v}')}{P(\mathbf{v})} \tag{1.15}$$

Thus the probability density ratio can be derived from the solution of the Fokker Planck equation as

$$P \sim f = exp\left(-\frac{m}{2D\gamma}\left(v - \bar{v}\right)^2\right) \tag{1.16}$$

where $\bar{v}$ is mean velocity.

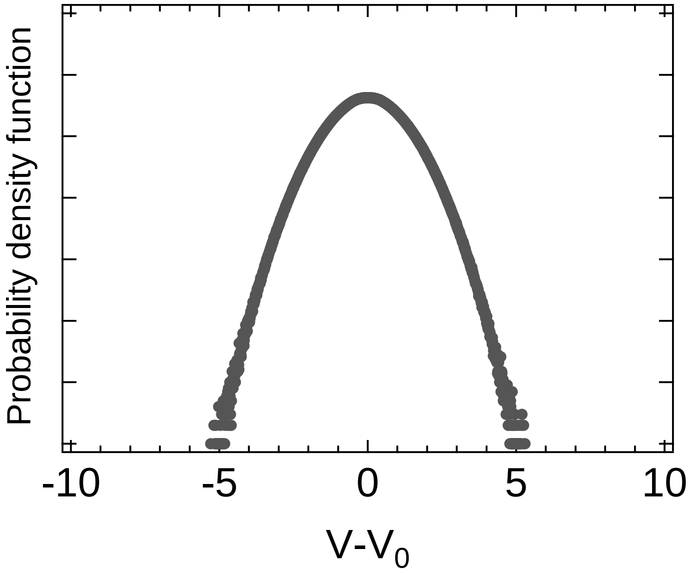

Figure 1.4: Monte Carlo Simulation example of the distribution of velocity using Metropolis algorithm by the principle of detailed balance on a semi-log scale

المنارة للاستشارات
www.manaraa.com

Another equilibrium of a stochastic probability $f(r, \mathbf{v}, t)$ in collisional term is a stochastic process given by

$$f(r_i, \mathbf{v}_i, t_i)f(r_j, \mathbf{v}_j, t_j) = f(r'_i, \mathbf{v}'_i, t'_i)f(r'_j, \mathbf{v}'_j, t'_j) \tag{1.17}$$

The entropy for a stochastic process is defined by

$$S = -kf \ln f \tag{1.18}$$

Above equilibrium, it has a granular jamming condition because of $\partial S/\partial t = 0$.

With a MC method, the velocity distribution is theoretically derived by the detailed balance and Metropolis-Hastings algorithm using the Langevin equation associated with the Fokker-Planck Equation. The jamming condition in granular dynamics driven by gravity may be approached in order to allow for a probability distribution.

1.1.3 Mass flow rate in hopper

Some pattern formation in the flow zone is proposed by Brown and Hawksley (1947). Kvapil (1959) described the flow of primary and secondary patterns. The primary pattern of granular materials is gravity driven and the secondary pattern performs on the aperture of the rapid flow. The discharge patterns are compared with funnel flow and mass flow by stagnant regions, Nguyen, T. (1979).

There are a number of methods to calculate mass flow rate from hoppers. The mass flow rate of pebbles through orifices was derived by Beverloo (1961) and Johanson (1965) for distinct types of mass flow and funnel flow. Figure 1.5 shows a schematic diagram of a conical hopper. The geometric parameters are the orifice size D_0, an angle α, and the diameter D of a cylindrical hopper.

www.manaraa.com

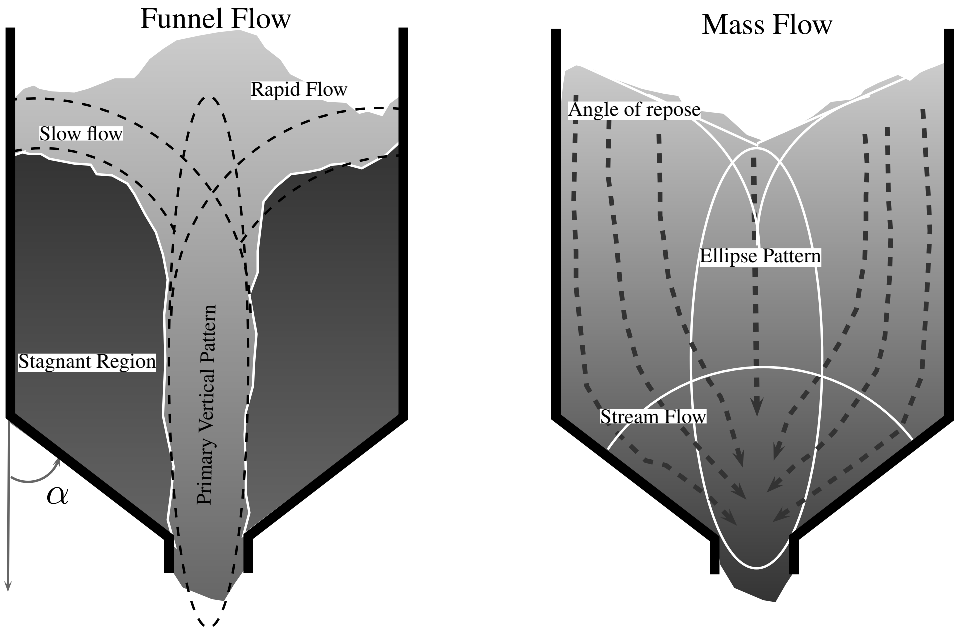

Figure 1.5: Schematic of a Pebble Bed Reactor showing vertical cross sections of a cylindrical vessel with a conical hopper: Left-side Beverloo (1961), Funnel flow and Right-side Johanson equation (1965), Mass flow

The Beverloo equation for the flow of rate W gives

$$W = C\rho\sqrt{g}\,(D_0 - kd)^{5/2} \tag{1.19}$$

where d is the diameter of pebble, k is a constant to be determined for a kind of particle and hopper properties (wall effect), ρ is packing density and C is a discharge coefficient to be determined experimentally from dissipation of inter-particle forces during contact.

The Johanson equation is derived from a semi-empirical model to predict the flow rate from mass flow.

$$W = A\rho\sqrt{\frac{D_0 g}{(1+m)\tan\alpha}} \tag{1.20}$$

المنارة للاستشارات
www.manaraa.com

where α is semi included angle of the hopper, ρ is packing density , A is a discharge coefficient and the value of m is one ($m = 1$) in a conical hopper.

1.2 Statistical Mechanics between the free volume function and the coordinate number

Pebble packing fraction can be investigated to determine the jamming or rocking condition in Pebble Bed Reactors with cylindrical cone shaped geometries.

The pebble bed volume fraction is $\phi = Nv_0/V$, where V is the fixed container volume and the pebble volume is $\pi d^3/6$, where d is diameter and N is the number of pebbles.

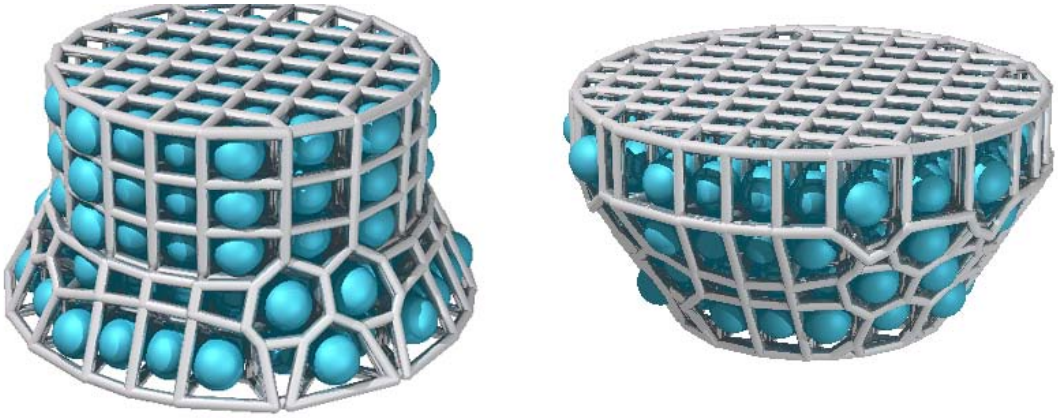

Figure 1.6: Voronoi diagram of modified source code voro++

The volume of the right cylindrical portion of the pebble bed is given by

$$V_c = \frac{\pi}{4} D^2 H_c \tag{1.21}$$

where D is the reactor diameter and H_c is the height of the cylindrical portion of the

المنارة للاستشارات
www.manaraa.com

pebble bed at the start of recirculation.

The volume of each conical portion of the pebble bed is given by the volume of a circular cone frustum and hence is

$$V_f = \frac{\pi}{12} H_f \left(D^2 + D_c^2 + DD_c\right) \tag{1.22}$$

where the vertical height H_f from the base cone angle mesured from the horizontal is the height between D_c and D.

The total volume is

$$V = \frac{\pi}{4} DH_c + \frac{\pi}{12} H_f \left(D^2 + D_c^2 + DD_c\right) \tag{1.23}$$

A different approach is to generate a Voroni diagram for the vertices plane between particle and their neighbor list dealing with the polyhedron. Calculations of edges of the intersection boundary are computed by the voro++ code, Rycroft, Grest, et al. (2006). The hopper shapes are modified to compute these Voroni diagram as shown in Figure 1.5.

Granular Structure Disorder plays a crucial role in statistical physics for the system of transportation in a phase transition. Recently, several important questions arose from Torquato and Stillinger (2010). In order to answer these questions, the family of volume fraction has not been classified by the parameters controlling a geometric structure. The geometric structure analysis presented the critical point at which a phase transition occurs. The critical point scale of the coordination number implies that changes in granular structure occur on a volume fraction. These methods are designed such that we can analytically develop a unified concept for the volume fraction and void fraction. It has been studied in simulations and experiments (Mehta, Barker 1991; Rintoul, Torquato

المنارة للاستشارات
www.manaraa.com

1996; Makse, Johnson, et al. 2000; Pugnaloni,Barker 2004; Zhang, Makse 2005; Aste 2006; Aste, Saadatfar, et al. 2006; Song, Wang, et al. 2008) where the phase transition can be inferred except for limited scale-up of packing fractions. In these cases, we have to deal with the whole system, which can be characterized in terms of granular ensemble originated by Edwards and Oakeshott (1989), which is defined from the configurations of ensembles in terms of the free volume function and compactivity. An important role of granular dynamics is to allow the volume fraction to be expressed in terms of the Kissing Number. Although a volume function exists on the macroscopic scale, the mesoscopic scale, and the microscopic scale, the main characteristics of the granular sphere packing fraction employs Random Loose Packing (RLP) (Epstein, Young 1962), Random Closed Packing (RCP) (Bernal, Mason 1960), Crystalline Structures, and the Kepler Conjecture. Under these circumstances, the sphere packing condition is indispensable and the critical coordination number of the degenerate system can provide direct access to the configurations. There are many previous theoretical and experimental results for N monosphere particles confined in a finite volume V. These methods are designed such that we can analytically develop a unified concept for the volume fraction and void fraction of interest.

To study one of the simplest granular systems, the volume function has been studied without answering the question of whether it is able to create consistence or not. We are developing a new theoretical approach to investigate the behavior of granular phase transitions. First of all, in this modeling approach, we allocate the free volume density function of the nearest coordinate number to delineate the parameters with physical interpretation. The analysis can be influenced by compactivity. The concept of a continuous volume function is employed until either the Kepler Conjecture, or RCP max is generated. It can be used to fit values and formulate the model equation and phase transition terms for physically reacting interactions of each particle of structured packing

www.manaraa.com

condition.

The free volume density function is defined in terms of the ratio of void fraction, ε to volume fraction, ϕ. $w \equiv \varepsilon/\phi$, the relation with $\varepsilon = 1 - \phi$ and $\phi = Nv_0/V$ with a single sphere volume v_0, and the number of particle, N limited the maximum free volume density value $w_k \approx 0.3505$ from the Kepler Conjecture, $\phi_k = \pi/\sqrt{18}$.

For a localized system, the free correction volume density function with the compactivity Γ, where the coordinate number z gives we should consider

$$\tilde{w} \equiv \frac{\varepsilon}{\phi} - \frac{\varepsilon_f}{\phi_f} = \frac{1}{\phi} - \frac{1}{\phi_f} \equiv \frac{1}{e^{\beta z - \alpha} - g(\Gamma)} \tag{1.24}$$

where $g(\Gamma)$ is the compression term and ϕ_f is the maximum volume fraction limit.

This distribution describes the correction volume function by the coordinate number. For states with mean coordinate number, where $e^{\beta z - \alpha} >> g(\Gamma)$ gives $\tilde{w} \approx e^{-\beta z + \alpha}$, and assuming $g(\Gamma) \approx 1$ and $e^{\beta z - \alpha} << 1$ using Taylor expansion gives $e^{\beta z - \alpha} \approx 1 + \beta z$ (when $\alpha = 0$) to $\tilde{w} \approx 1/\beta z$, these approximation methods agree to the inverse of the coordination number (Aste, 2006; Aste, Saadatfar et al. 2006; Song, Wang et al. 2008). We found the value $\beta^{-1} = 2\sqrt{3}$ with the data k value from Song, Wang et al. 2008, but their value is from numerical regression, while $\phi \to 0$, $\tilde{w} \to \infty$ and $\phi \to \infty$, $\tilde{w} \to 0$ correspond in the present treatment.

Solving the volume density function yields

$$z = z_c + k \ln\left(1 - \Gamma + \frac{1}{1/\phi - 1/\phi_f}\right) \tag{1.25}$$

where the critical coordination number $z_c = \alpha/\beta$, $k = 1/\beta$ and $g(\Gamma) = 1 - \Gamma$.

Figure 1.7 (top) shows the free volume density function vs the coordinate number diagram. In a portion of the plane between $z = 4$ to $z = 6$ in the RLP-RCP line,

المنارة للاستشارات
www.manaraa.com

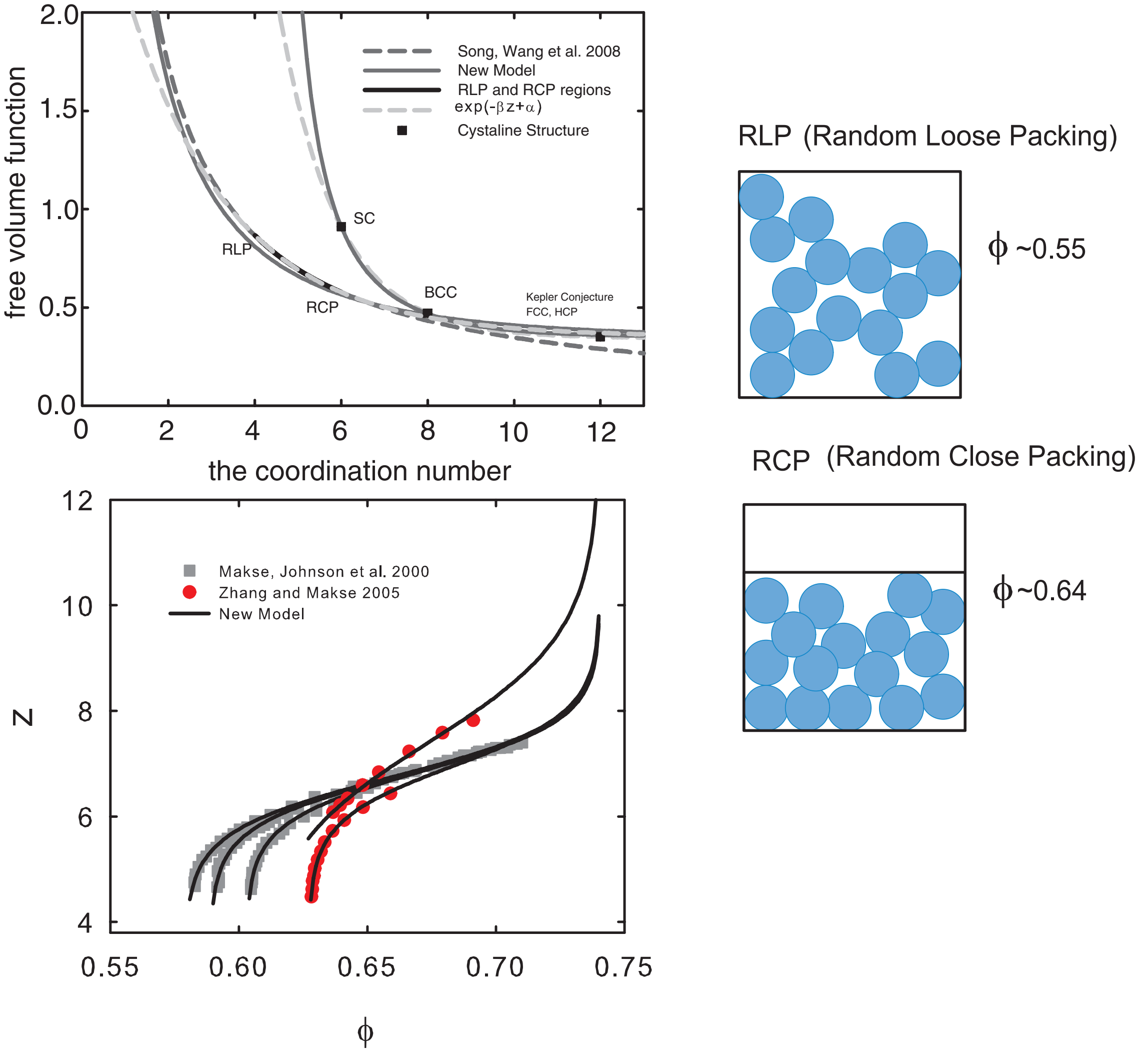

Figure 1.7: The coordinate number and free volume function in the New Model region (top), and the data of Makse, Johnson 2000; Zhang, Markse 2005 fitted by the New model (bottom), also the configuration of RLP and RCP

www.manaraa.com

Wang's data and the new model are identical. We could provide a reasonable statistical interpretation, of evidence, to a critical coordination number of one sort. Certainly, we determine the various ranges to divide into the two classes of frictionless and frictional spheres along with the mean coordination number. For frictional spheres, the original data are taken from references listed as shown in Figure 1.7 (bottom). Equation (1.25) was fit to the data to determine the mean value in good agreement with frictional $z_c = 4$. At the level of a different compression rate, the prediction line beyond the data corresponds to the limit of maximum packing fraction (Kepler Conjecture). The mean coordination number of frictionless $z_c = 6$ is in good agreement with a previous result (Mehta, Barker 1991) in accordance with increasing Γ. Investigation of the transition of granular dynamics to the existence of an essentially volume free function and localized critical coordination numbers was also performed. The equation of such highly nonlinear structures fits experimental data shows the fundamental interest and possible relevance to the jamming transition (Appendix A).

المنارة للاستشارات
www.manaraa.com

Chapter 2

Theory and Analysis

2.1 Euler–Lagrange Dynamics for granular systems

A Molecular Dynamics (MD) Simulation is based on Newton's second law on time evolution within the framework of classical mechanics. The motion of granular dynamics can be described by Euler-Lagrangian dynamics. From a comprehensive point of view, the Euler-Lagrangian dynamics is presented to clearly and easily identify the pair interaction and contacting time among the individual particles. The kinetic energy and the potential energy are used to obtain the Lagrangian of the particle with the generalized coordinate and its associated granular interaction term. In this work, the system of N particles was the only constraint used to move the particles through the external gravitational force and the energy dissipated in friction. The MD simulation or Discrete Element Method (DEM), originally proposed by Cundall and Strack (Cundall and Strack 1979), has been developed and used as a critical numerical tool to simulate granular dynamics. The theory becomes very complex for an analytical solution when a large number of bodies are involved within the system. However, for the purpose of explaining the phenom-

المنارة للاستشارات
www.manaraa.com

ena, classical interactions of thermodynamics and statistical mechanics are often used to characterize properties of the system. The molecular dynamics categorized as DEM for granular dynamics can be used to represent the soft particles of the PBRs because the kissing particles are allowed to overlap during the contract time. Thus, the system considers nonconservative forces from friction. To simulate MD, previous work was required to explain the forces through analyzing the energy distribution. Lagrangian dynamics generally states that the pebble's motion, which describes the transitional motion of the center of mass and the rotational motion about the center of mass, has non-conservation of the frictional force. Consequently, this form of Lagrange's equation represents the underlying interaction and therefore becomes advantages. This approach can easily describe the system.

For a granular system of N particles moving in three dimensional space with constraints, D'Alembert's principle requires knowledge of the constraint forces, (typically and static), kinetic frictional force and particle sliding. What was needed was a description of the system that makes compromises when dealing with the constraint relations. D'Alembert's principle provides such a description for systems involving holonomic or nonholonomic constraints in allowing virtual displacements, $\delta\mathbf{r}_i = \sum\limits_a \frac{\partial \mathbf{r}_i}{\partial q_a}\delta q_a$ in contrast with a real displacement $d\mathbf{r}_i$. There are two types of constraints. The first one is holonomic constraints which can be solved for using kinematics; here there is no work ($\mathbf{F}_i^{(c)} \cdot \delta\mathbf{r}_i = 0$) because virtual displacements $\delta\mathbf{r}_i$ are orthogonal to the corresponding constraint forces $\mathbf{F}_i^{(c)}$. The second is nonholonomic constraints which must be solved for using dynamics; here consequently we have a work term ($\mathbf{F}_i^{(c)} \times \delta\mathbf{r}_i \neq 0$).

As a consequence of these constraint relations, this problem is solved by choosing Lagrange's equation. The Euler–Lagrange equations, $L\left(q_a, \dot{q}_a\right)$ in the generalized coor-

المنارة للاستشارات
www.manaraa.com

dinates, q_a for a discrete system is

$$\frac{d}{dt}\frac{\partial L}{\partial \dot{q}_a} - \frac{\partial L}{\partial q_a} = Q_a \tag{2.1}$$

Here $L \equiv T - V - U$ is the Lagrangian of the system.

The generalized constraint forces, Q_a are derived from D'Alembert's principle for the virtual work for applied forces. Two nonconservative components are associated with respect to $\dot{q}_a$ and q_a. The generalized constraint forces on the right-hand side are given by

$$Q_a \equiv \mathbf{F}_{ij}^{(c)} \cdot \frac{\partial \mathbf{r}_{ij}}{\partial q_a} = \mathbf{F}_{ij}^{(f)} \cdot \frac{\partial \mathbf{r}_{ij}}{\partial q_a} - \frac{\partial \mathcal{F}}{\partial \dot{q}_a} \tag{2.2}$$

where $\mathbf{F}_i^{(f)}$ is only for the friction force and $\mathcal{F}$ is known as Rayleigh's dissipation function $\mathcal{F} = \frac{1}{2}\sum\limits_{a,b} c_{ij}\dot{q}_a\dot{q}_b$ (if $c_{ij} = c_{ji}$, the symmetric tensor).

The Lagrange equation with Rayleigh's dissipation function and contact friction becomes

$$\frac{d}{dt}\frac{\partial L}{\partial \dot{q}_a} - \frac{\partial L}{\partial q_a} + \frac{\partial \mathcal{F}}{\partial \dot{q}_a} = Q_a^{(f)} \tag{2.3}$$

where $Q_a^{(f)} = \mathbf{F}_{ij}^{(f)} \cdot \frac{\partial \mathbf{r}_{ij}}{\partial q_a}$. The generalized constraint force is presented by a frictional force.

In the case in which particles were assumed to be the spherical rigid bodies located in the gravitational field, the generalized coordinates were decoupled into the center of mass coordinates (the axes of the inertial coordinate system) and the Euler angles (θ, ϕ, ψ). Since the spherical rigid body is symmetrical for the Euler angles, the moment of inertia for an ideal homogeneous sphere of radius R is $I = \frac{2}{5}mR^2$ is about the principal axis

www.manaraa.com

of the center of mass. From the relations above we can compute one term relating the kinetic energy T of the translational motion and the spin rotation itself about the center of mass. Another term relating the potential energy of the gravity potential V and a pairwise interaction potential $U(r_{ij})$, is given where the distance between the centers of the two particles is $r_{ij} = |\mathbf{r}_i - \mathbf{r}_j|$ with respect to a fixed frame and $\mathbf{r}_i$, $\mathbf{r}_j$ is the relative position vector of the center of mass m_i, m_j.

The distance between particles i and j about a fixed point O, the relative position about the normal and tangential direction, is independent. Above all, the relative angular velocity in the rotating frame is contributed to the angular displacement from the equation

$$\omega_i \times \frac{R_i}{R_i + R_j}\mathbf{r}_{ij} + \omega_j \times \frac{R_j}{R_i + R_j}\mathbf{r}_{ij} = \omega_{ij} \times \mathbf{r}_{ij} \tag{2.4}$$

The relationship of the overlap displacement is defined as

$$\delta r_{ij} = \left(\hat{\mathbf{r}}_{ij} \cdot \delta_{ij}\right)\hat{\mathbf{r}}_{ij} + \hat{\mathbf{r}}_{ij} \times \left(\delta_{ij} \times \hat{\mathbf{r}}_{ij}\right) - \int \omega_{ij} \times \hat{\mathbf{r}}_{ij} d\tau \tag{2.5}$$

Here the center of angular velocity is $\omega_{ij} \equiv \left(R_i\omega_i + R_j\omega_j\right)/\left(R_i + R_j\right)$, with angular velocities ω_i and ω_j in a rotating coordinate frame with each particle at the center of mass of the system during contact time t_c.

The relative normal displacement is

$$\delta r_{ij\|} = \left(\hat{\mathbf{r}}_{ij} \cdot \delta_{ij}\right)\hat{\mathbf{r}}_{ij} \tag{2.6}$$

www.manaraa.com

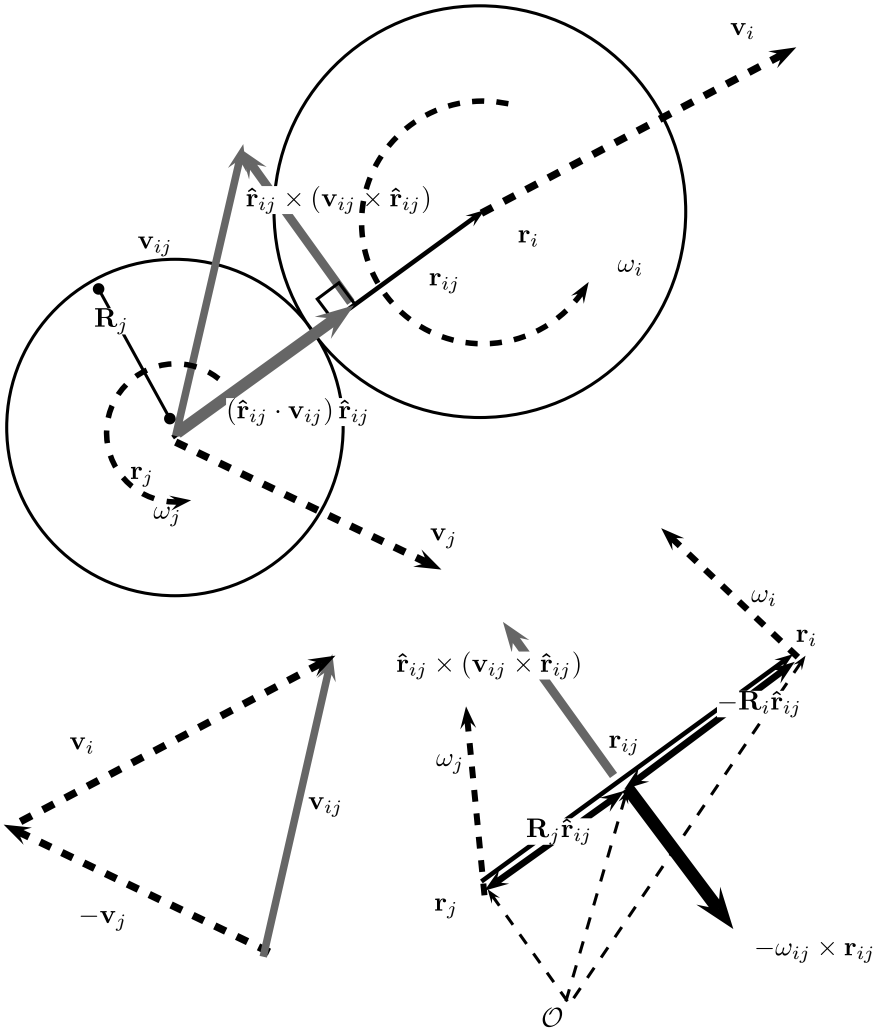

Figure 2.1: Schematic of the vector analysis contacting on particle acting $j \rightarrow i$

المنارة للاستشارات
www.manaraa.com

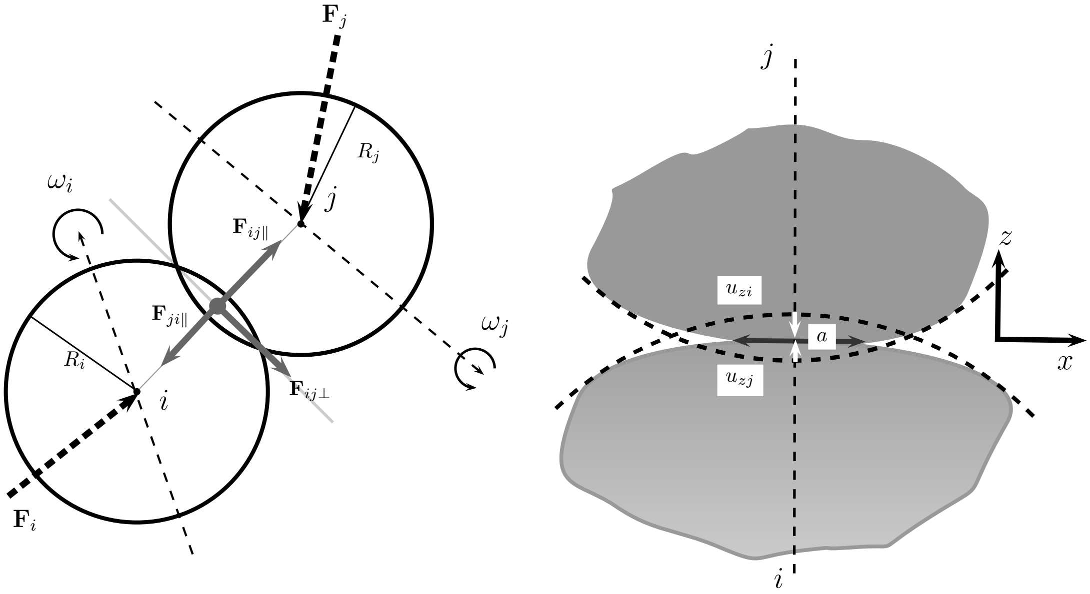

Figure 2.2: Schematic of the interaction between two particles at contact with position vectors $\mathbf{r}_i$, $\mathbf{r}_j$: The left figure of a set of a overlap shape and the right figure of the deformable shape of Hertz-Mindlin force

and the relative tangential displacement is

$$\delta r_{ij\perp} = \hat{\mathbf{r}}_{ij} \times (\delta_{ij} \times \hat{\mathbf{r}}_{ij}) - \int_{t_c} \omega_{ij} \times \hat{\mathbf{r}}_{ij} d\tau \tag{2.7}$$

A comparison with the above gives the relative velocity as

$$\begin{aligned} \left.\frac{d\mathbf{r}_{ij}}{dt}\right|_s &= \dot{\mathbf{r}}_{ij} - \omega_{ij} \times \mathbf{r}_{ij} \\ &= (\hat{\mathbf{r}}_{ij} \cdot \mathbf{v}_{ij})\,\hat{\mathbf{r}}_{ij} + \hat{\mathbf{r}}_{ij} \times (\mathbf{v}_{ij} \times \hat{\mathbf{r}}_{ij}) - \omega_{ij} \times \mathbf{r}_{ij} \end{aligned}$$

where $\hat{r}_{ij} = \mathbf{r}_{ij}/r_{ij}$ and $\mathbf{r}_{ij} = \mathbf{r}_i - \mathbf{r}_j$, the relative velocity in term of j.

المنارة للاستشارات
www.manaraa.com

The relative velocity $\dot{\mathbf{r}}_{ij} = \mathbf{v}_{ij} = \mathbf{v}_i - \mathbf{v}_j$ has the components of the relative normal displacement

$$\mathbf{v}_{ij\parallel} = (\hat{\mathbf{r}}_{ij} \cdot \mathbf{v}_{ij})\, \hat{\mathbf{r}}_{ij} \tag{2.8}$$

and the relative tangential velocity is given by

$$\mathbf{v}_{ij\perp} = \hat{\mathbf{r}}_{ij} \times (\mathbf{v}_{ij} \times \hat{\mathbf{r}}_{ij}) - \omega_{ij} \times \mathbf{r}_{ij} \tag{2.9}$$

where $\hat{\mathbf{r}}_{ij} \times (\mathbf{v}_{ij} \times \hat{\mathbf{r}}_{ij}) = \mathbf{v}_{ij} - (\hat{\mathbf{r}}_{ij} \cdot \mathbf{v}_{ij})\, \hat{\mathbf{r}}_{ij}$.

When granular particles have pairwise collisions, they collide instantly and have an infinitesimally small time for the Hertz's potential. This impulse imparts interactions between each particle. Figure 2.2 shows analytic geometry, before instantaneous deformation, at which point the bodies touch at an adjacent point. The curvatures of the two bodies are represented with radii of curvature R_i and R_j. At the contact area, the bodies are compressed with smooth curvature. The shape of the particle is changed by the curvature due to the elastic restoration force. Previously, Hertz's theory had been used with a quadratic equation. However, contact pressure provides displacement under the surface. This contact pressure is distributed throughout the curvature. The pressure distribution function acts at each contact radius a. The distribution of normal stress in the contact area as a function of distance was also reported (Johnson 1985). The granular particles behave like hard sphere which contact one another with a deformable contact force. The forces between the two particles can be approximated well by Hertz theory of elasticity. The granular interaction potential is a power law from Hertz theory. Hertz contact is presented to determine each granular surface interaction for granular flows. The generalized expression for the normal contact force acting on a granular body, in which the governing equation is either loaded in tension or in compression, is obtained

المنارة للاستشارات
www.manaraa.com

from the stress and strain relation of the material. The Hertz potential is derived from the results of stress-strain analysis that are attributed to granular flow sensitivity. Granular particle interactions have a virtual depth in the relation with a remarkable normal contact of relative deformation in terms of a tangential contact by a friction on a contact surface. A substantial solution to the problem of a normal contact has been known as Hertz's theory.

We are led to the relations of the overlap displacement as defined by δr_{ij} where the normal displacement $\delta r_{ij\|} \equiv R_i + R_j - |\mathbf{r}_i - \mathbf{r}_j|$ is the depth of indentation or normal overlap for the contact between the two bodies of radii R_1 and R_2. When $\delta r_{ij\|} > 0$, a contact force is generated that otherwise would have zero potential. The noncohesive granular interaction is described by Hertz-Mindlin potential between particles,

$$U\left(r_{ij}\right) = \frac{2}{5} k \delta r_{ij}^{5/2} \tag{2.10}$$

where $k_n = \frac{4}{3} E^* \sqrt{R^*}$ is the stiffness of the pairwise interaction proposed in Hertz theory (Hertz 1895) and the tangential term $k_t = 8G^* \sqrt{R^*}$ is the tangential force (Mindlin 1949) with the effective Radius $R^* = R_i R_j / \left(R_i + R_j\right)$ and the effective Young's modulus $E^* = \left(\frac{1-\nu_i^2}{E_i} + \frac{1-\nu_j^2}{E_j}\right)^{-1}$, E the Young's modulus and the effective Shear modulus is $G^* = \left(\frac{2(2-\nu_i)(1+\nu_i)}{E_i} + \frac{2(2-\nu_j)(1+\nu_j)}{E_j}\right)^{-1}$. Poisson's ratio is ν for the contacting particle i and j respectively (Brilliantov, Spahn et al. 1996; Silbert, Ertas et al. 2001, Zhang and Makse 2005).

Comparisons of this with the Lagrangian obtained previously can be expressed by the gravitational potential

$$V\left(r_i\right) = m_i \mathbf{r}_i \cdot \mathbf{g} \tag{2.11}$$

www.manaraa.com

where $\mathbf{g}$ is the gravitational acceleration vector.

The pair dissipative function can be derived from Rayleigh's dissipation function

$$\mathcal{F} = \frac{1}{2}\gamma m^{*}\delta\dot{r}_{ij}^{2} \tag{2.12}$$

where γ is a dissipative constant or viscous damping coefficient given a coefficient of normal restitution e for a contacting time with normal and tangential contact.

When the particle i is moving to another particle j at contacting time, it follows that the force of constraint exerted by kinetic friction (μ_k, the kinetic coefficient of friction) of each particle has done real work after the collision. Thus the virtual displacement, $\delta\mathbf{r}$, is tangent to the other particle and orthogonal to the constraint force. If both particles are at a rest state ($\mu_s \leq \mu_k$), the sphere at contact experiences the only force on the pebble from the static friction (μ_s, the static coefficient of friction) which is perpendicular to the curved part of particle. The normal and tangential direction is independent, and then each term must be separate. The motion of the ith particle is given by a contact force and a damping force during collisions. If the tangential force is generated, the generalized constraint force is $Q_a^{(f)} = -sign\left(\delta r_{ij\perp}\right)\min\left(\mu\left|\mathbf{F}_{ij\parallel}\right|, \left|\mathbf{v}_{ij\perp}\right|\right)\hat{\mathbf{r}}_{ij\perp}$.

Thus, the Lagrange's equation of the net binary system can be expressed in term of r_{ij}

$$L = \frac{1}{2}m^{*}\left|\delta\dot{r}_{ij}\right|^{2} - U\left(r_{ij}\right) \tag{2.13}$$

where $m^{*} = m_i m_j/\left(m_i + m_j\right)$ is the reduced mass of the system.

As a consequence of the decoupling, the Lagrange equations of motion separate into two equations, one for the center of mass coordinates and another for the Euler angles. Each set can be analyzed independently to apply this prescription to a two body problem

www.manaraa.com

for a virtual displacement. The present simulations use a normal and tangential contact model comprised of the following:

$$\left|\delta\dot{r}_{ij}\right|^2 = \left|\delta\dot{r}_{ij\parallel}\right|^2 + \left(1+\frac{1}{\zeta}\right)\left|\delta\dot{r}_{ij\perp}\right|^2 \tag{2.14}$$

where $\zeta = \left(\frac{1}{m_i\tilde{I}_i} + \frac{1}{m_j\tilde{I}_j}\right)^{-1}$ from the particle moment of inertia $\tilde{I}_i = I_i/m_iR_i^2$ and $\tilde{I}_j = I_j/m_jR_j^2$ about the torque acting on two particle.

Finally, we can implement Euler-Lagrangian dynamics to find out the governing equation and contact time used to simulate the MD method. Although the theoretical approach is Hertz's contact to the Lagrangian solution, problems arise including general friction through contacting area where $\mathbf{F}_{ji} = -\mathbf{F}_{ji}$, Newton 3rd law and the tangential component $\mathbf{F}_{ij\perp}$ and $\delta r_{ij\perp}$ which can be described to meet the requirement of Coulomb yield criterion if $|\mathbf{F}_{ij\perp}| < \mu_s\mathbf{F}_{ij\|}$. Until the particles are separated, the potential calculation is performed for the interaction only once on each pair of particles. The equations of motion follow directly from the Lagrangian formulation described above.

The normal component of the contact force can be written as

$$\mathbf{F}_{ij\|}{=}k_n\delta r_{ij\|}^{3/2} - \gamma_n m^*\mathbf{v}_{ij\|} \tag{2.15}$$

The shear component of the contact force can be written as

$$\mathbf{F}_{ij\perp} = -k_t\sqrt{\delta r_{ij}}\delta r_{ij\perp} - \gamma_t m^*\mathbf{v}_{ij\perp} \tag{2.16}$$

The equation of motion will be expressed in normal and tangential directions on contact condition, $|\mathbf{F}_{ij\perp}| > \mu_s\mathbf{F}_{ij\|}$, $\mathbf{F}_{ij\perp} = -\mu_k\mathbf{F}_{ij\|}\hat{\mathbf{v}}_{ij\perp}$ and $\gamma_t m^*\mathbf{v}_{ij\perp}$ which generates the rolling friction from the center of particle j to the center of particle i. This component

www.manaraa.com

in the direction of motion is attributed by performance of the Hertz-Mindlin theory to improve the terms of the tangential force. The simulation will demonstrate the essential results of the contact deformable interaction. Two body forces are represented by the potential, which is enough to permit the surface effects. The governing equation, constructed from two-body functions, is applied to the many body system problem with a contact dynamic using a MD simulation (or DEM).

2.2 A Compressible Kinematic Model for Particle Flow in Pebble Bed Reactors

Granular dynamics of pebbles in a Pebble Bed Reactor (PBR) is very complex due to many body interactions as well as the long range interactions that arise from stress fields. Of particular interest in a PBR is the arching or locking phenomenon, which hinders the ability of the fuel pebbles to drain out during refueling. In general, driven granular flow is governed by the geometry and external boundary conditions of silos and hoppers, and material properties such as contact friction and elasticity. Evidently, a firm understanding of the pebble flow mechanisms plays an important role for a robust design of a Pebble Bed Reactor.

A natural way to describe granular motion is through the continuum approach where the grains are not thought to be composed of discrete particles but rather, they are treated as continuously filling the region they occupy. In this section, we propose a new kinematic model for granular flow that explicitly accounts for changes in the density field. The present model combines the compressible continuity equation and the phenomenological velocity relationship developed by Nedderman and Tüzün (1979) for free-flowing granular flows. Approximate solutions of this model show that finite density variations result in

المنارة للاستشارات
www.manaraa.com

non-Gaussian velocity profiles. This observation is consistent with several experimental data on controlled granular flow (Beverloo, Leniger, et al. 1961; Choi, Kudrolli, et al. 2004; Choi, Kudrolli, et al. 2005). Our preliminary results thus indicate that the density field can play an important role in granular flow dynamics and may have an effect on pebble jamming in a PBR during refueling.

An analytic approximate solution of the Semi-Empirical New Kinematic Model with the boundary conditions is developed for a compressible packing condition. It is based on the velocity description of the packing density in hopper. The packing structure can represent the jamming phenomenon by its flow types. The analytical formulas for the quasi-linear diffusion and convection coefficients of the velocity profile are obtained. In an attempt to say precisely what a velocity distribution is, the probabilistic interpretation is used to describe the macroscopic quantities such as density, flux, mean velocity, and void fraction etc. In the kinematic model proposed by Nedderman and Tüzün (1979), it is assumed that the transverse velocity is proportional to the gradient of the vertical velocity as shown below

$$\mathbf{v}_{\perp} = -b\nabla_{\perp}v_z \tag{2.17}$$

where the total velocity is defined as the vector sum of transverse and vertical components ($\mathbf{v} \equiv \mathbf{v}_{\perp} + \mathbf{v}_z$), and dissipation in collisions is described by means of a parameter which is related to the coefficient of diffusion length b. The empirical constant can be used for determining a calibration and validation of any model in a macroscopic velocity field with the limitation to the kinetic energy that is lost in collisions and shear flow.

These parameters may depend on the vertical height from the hopper and the boundary conditions. The reason for this inconsistency problem centers on the experimental

www.manaraa.com

interpretation of Gaussian distribution. The velocity flow adjacent to the wall of left and right boundaries is physically constrained to flow parallel or tangent on the wall. If the velocity vector is tangent, then its normal component must clearly be zero. If the Neumann boundary condition is replaced by the requirement that the derivative of the velocity be zero at the edges on the wall, $\mathbf{v} \cdot \hat{n} = 0$, where $\hat{n}\,(\equiv \nabla\Omega/\left|\nabla\Omega\right|)$ is normal direction to the surface Ω function of the wall.

When combined with the incompressible continuity condition, $(\nabla \cdot \mathbf{v} = 0)$, the phenomenological model given by Equation(2.17) results in a diffusion-type equation for the vertical velocity. The solution, which is a Gaussian, compares favorably to experimental data from free-flowing granular systems. However, small non-Gaussian deviations are observed for slow granular flows and closer to the drainage orifice.

In this section, it is proposed that the pebble density field can introduce a perceptible change to the granular flow dynamics. In our new model, a compressible continuity condition $\nabla \cdot (\rho\mathbf{v}) = 0$ is introduced along with the constitutive equation given by Equation(2.17). This results in the following convection-diffusion equation:

$$\frac{\partial v_z}{\partial z} = \nabla_\perp \cdot (b\nabla_\perp v_z) + \frac{\nabla_\perp \rho}{\rho} \cdot b\nabla_\perp v_z - \frac{1}{\rho}\frac{\partial \rho}{\partial z} v_z \tag{2.18}$$

where ρ is the density field, not a single particle density. Note that the compressible model has convection terms that arise from the gradients in the density. The above equation can be solved exactly if the density variations are considered to be weak. For this purpose we define two parameters λ and κ as

$$\lambda \equiv \frac{\partial b}{\partial x} + \frac{b}{\rho}\frac{\partial \rho}{\partial x} \text{ and } \kappa \equiv -\frac{1}{\rho}\frac{\partial \rho}{\partial z} \tag{2.19}$$

Equation (2.18) now can be expressed (in two dimensions, the radial spatial variable

www.manaraa.com

x and z) as

$$\frac{\partial v_z}{\partial z} = b\frac{\partial^2 v_z}{\partial x^2} + \lambda\frac{\partial v_z}{\partial x} + \kappa v_z \tag{2.20}$$

A solution to the above equation is

$$v_z = \exp\left[\left(\kappa - \frac{\lambda^2}{4b}\right)z - \frac{\lambda}{2b}\right]u\left(x, z\right) \tag{2.21}$$

where $u\left(x, z\right)$ satisfies the auxiliary parabolic equation

$$\frac{\partial u\left(x, z\right)}{\partial z} = b\frac{\partial^2 u\left(x, z\right)}{\partial x^2} \tag{2.22}$$

Now with $v_z = f\left(x, 0\right)$ at $z = 0$, the equation is

$$u\left(x, 0\right) = f\left(x\right)\exp\left(\frac{\lambda}{2b}x\right) \equiv g\left(x\right) \tag{2.23}$$

For the domain $-\infty < x < \infty$, we can write the solution formally as:

$$u\left(x, z\right) = \int_{-\infty}^{\infty} g\left(\xi\right)\exp\left(\frac{\lambda}{2b}x\right)G\left(x, \xi, z\right)d\xi \tag{2.24}$$

where the kernel G is given by:

$$G\left(x, \xi, z\right) = \frac{1}{\sqrt{4\pi bz}}\exp\left[-\frac{\left(x - \xi\right)^2}{4bz}\right] \tag{2.25}$$

If $g\left(x\right) = Q\delta\left(x\right)$ where Q is a constant flow rate which is proportional to mass flow rate at an orifice (initial condition), the solution for u is given by the following Gaussian expression

www.manaraa.com

$$u\left(x,z\right) = \frac{Q}{\sqrt{4\pi bz}} \exp\left[-\frac{x^2}{4bz}\right] \tag{2.26}$$

The final solution for the pebbles' vertical velocity field (with an additional symmetric condition imposed at $x = 0$) is given by:

$$v_z = \frac{Q}{\sqrt{4\pi bz}} \exp\left[\left(\kappa - \frac{\lambda^2}{4b}\right) z\right] \exp\left(-\frac{x^2}{4bz}\right) \tag{2.27}$$

Vertical velocity profiles with the Nedderman and Tüzün kinetic model (old, middle curve) and the new compressible kinetic model (positive and negative κ) at two different vertical (z) locations (z=4, z=10) as shown in Figure (2.3). λ and κ are small parameters in the new model. Notice the non-Gaussian deviations with relatively small density variations.

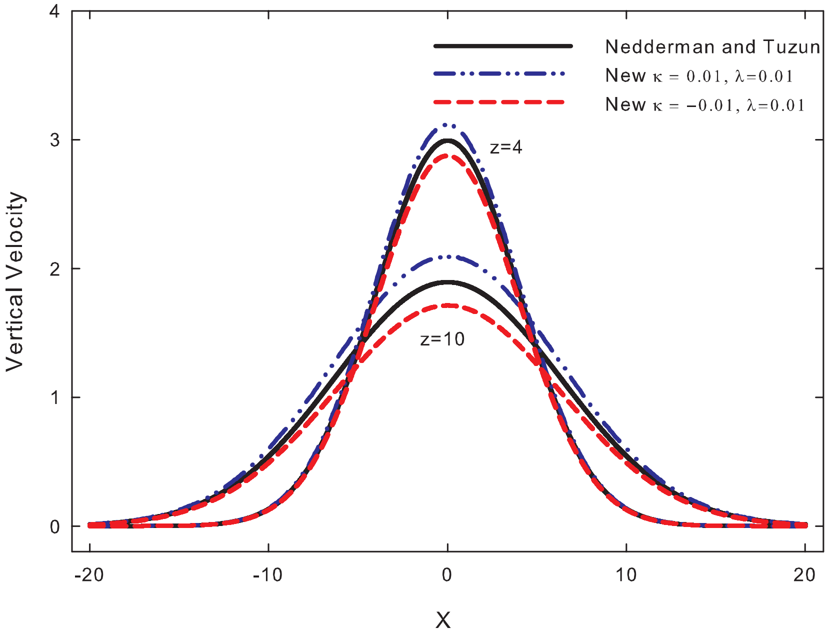

Figure 2.3: The effect of λ and κ on the vertical flow profile

www.manaraa.com

There are several interesting features for the compressible flow solution. We can first note that when λ and κ are identically equal to zero, the solution collapses to the Nedderman and Tüzün Gaussian profile. Changes in density are reflected through the additional (first) exponential term. Recall that λ and κ are the density gradients in z and x directions, respectively (assuming b is constant). Since λ and κ can be regarded as small parameters in the first approximation, the effect of density gradient in the transverse direction (x) is small compared to that in the vertical direction (z). Kinematic models, as mentioned before, are successful for free-flowing fast granular flows. When the drainage flow becomes weaker, the effect of density variations (and the attendant locking and arching phenomena) can become prominent. In a PBR, the pebble flow is intermittent and a central challenge is to characterize the flow fields in such intermittent conditions. With a Compressible Kinematic Model designed for a packing density, the velocity profile is theoretically derived by the compressible packing condition. The vertical velocity is influenced by the term of λ and κ. In solving variable coefficients, the problem may be approached to allow a packing density distribution which is a packing structure by density to explain the jamming phenomenon. We have initiated an approach based on Molecular Dynamics Simulation or Discrete Element Methods for characterizing the pebble flow conditions in a PBR during refueling.

المنارة للاستشارات

www.manaraa.com

Chapter 3

Simulation

Classical Molecular Dynamics (MD) simulations have been performed using the Large-scale Atomic/Molecular Massively Parallel Simulator (LAMMPS) and an additional simulation of LAMMPS Improved for General Granular and Granular Heat Transfer Simulations (LIGGGHTS). These codes are based on the Open Source MD code written in C/C++ language of the time evolution of the simulating system in the velocity Verlet algorithms (or Gear predictor-corrector algorithm) in the 3-dimensional space. MD simulation (or DEM) algorithm is used to determine the position, the velocity, and the acceleration from the initial positions and velocities. The translational and rotational equation of each particle from total force and total torque are given by

$$\frac{\partial^2 \mathbf{r}_i}{\partial t^2} = \frac{\mathbf{F}_i}{m_i} \text{ and } \frac{\partial^2 \omega_i}{\partial t^2} = \frac{\tau_i}{I_i} \tag{3.1}$$

The accelerations, velocities and displacements are updated from the previous time-step using a time integration scheme. It is assumed now that the evolution in time of the considered system includes the neighboring cell because it is within the cutoff radius (r_{cut}), where $r_{ij} < r_{cut}$. At each time step, the positions r_i of the force on cutoff range

المنارة للاستشارات
www.manaraa.com

is neglected as $\mathbf{F}_{cutoff} \cong 0$ which leads to much faster precessing for computational efficiency.

It has been used successfully to demonstrate that pairwise interaction between particles is described by the Hertz-Mindlin contact forces as a dynamic processing and the time evolution in three dimensions (3D). Bulk solid motion of many particles is a discontinuous phenomenon that requires statistical analysis. By using the results of numerical simulations, the data visualization approach (ParaView) provides a sophisticated concept to be comprehended more clearly by granular characteristics. Before computational simulation, the simulation design is associated with the scale up of the Pebble Bed Reactor in order to ensure the safety analysis. The reactor geometry enables further detailed information to be obtained which is relevant to measure radioisotope particle tracking.

3.1 Design and Scale up for Pebble Bed Reactors

Pebble Bed Reactors (PBRs) implement the scale-up properties when accounting for a type of very high temperature reactor (VHTR). The density transmission gauges can be calculated by the maximum length between the source and detector response. This is based on the radiation attenuation in the pebbles granular material where the reactor container is included within its associated packing fraction. Once the evaluation of PBRs diameter is carried out, a gauge transmission of the gamma-ray radioisotope tracer is implemented. This method is used to quantitatively analyze the two phase (gas-pebbles) mixture and a transmitted peak counting rate which is determined by our Forward Scattering Gauge Model (FSGM). FSGM uses the mixture attenuation coefficient of the packing from a single characteristic photon. The source is an isotropic gamma ray source

www.manaraa.com

of Cs 137 with an activity of $10\mu Ci$ at 662 keV. The spectrum of a 2×2 Nal(Tl) detector is taken to account for the total number integrated single photopeak according to the detection response with full-energy-peak efficiency. Effective and maximum scale can be determined using a relative approach with/without pebbles. The approach is based on using transmission techniques to measure the density thickness and the error analysis can be obtained from an associated accurate length prediction. The limitation is that the sensitive mass attenuation coefficient becomes difficult as to the composition of reactor's alloy in pursuit of the interest region shape, as in the case of the hopper. This preliminary assessment allows us to make PBRs configurations with the critical scale-up conditions. The main results are derived from FSGM, where a scale uncertainty is taken into consideration. For the size of pebble diameter, the discrete displacement is indicated to cognize the detection resolution.

The Forward Scattering Gauge Model (FSGM) shows that the optimum design criterion is based on the minimum relative thickness error, $\sigma(t)/t$. The corresponding counting rate of the γ-rays is represented by Lambert-Beer's law

$$R\left(t\right)=f_{mix}R_0\exp\left(-2\mu_w w-\mu_{mix}t\right) \tag{3.2}$$

Where $R\left(t\right)$ is the gauge response for inner diameter t in dps(Bq) as substituting in terms of $\mu_{mix}=\mu_g\epsilon+\mu_p\phi$, where μ_{mix} mix is the linear attenuation coefficient and ϵ and ϕ are the volume fraction of gas and pebbles, respectively $(1=\epsilon+\phi)$, and μ_w is the linear attenuation coefficient of the wall and w is thickness of wall on the cylindrical vessel wall and R_0 is the source strength. f_{mix} is the detector efficiency factor, that the counting yield can be expressed as the product of several independent detection parameters: Cs-137, 0.86 branching ratio to 662 keV, NaI(Tl) 2×2 detection efficiency $=0.9$, photopeak

المنارة للاستشارات
www.manaraa.com

efficiency = 0.5, and geometric solid angle= $\pi r^2/4\pi t^2$.

Then inner diameter t, between source and detector, shows its results below:

Table 3.1: Detector response results using FSGM

inner diameter t	the ratio of response	counting rate (cps)
50cm	7.64×10^{-7}	2.83×10^{-1}
100cm	4.39×10^{-10}	1.62×10^{-10}

The standard deviation of the distance measurement $\sigma(t)$ is given in terms of the standard deviation of the gauge response $\sigma(R)$ as

$$\sigma(t) = \sigma(R)/\left(\frac{\partial R}{\partial t}\right) \tag{3.3}$$

Where $\sigma(R) = \sqrt{R/\tau}$ is given by Poisson statistics and τ is the time over which the gauge response is taken. Finally, returning to the original variables:

$$\frac{\partial \sigma(t)}{\partial \mu_{mix}} = 0 \tag{3.4}$$

Thus, the optimum conditions are found to be given by $\mu_{mix} t = 2$, when the volume fraction of marbles is 0.6 and the reactor's diameter is 18 cm.

The benchmark calculations of previous PBRs in table 3.2 (Gougar, H. D., A. M. Ougouag, et al. 2004) presented the basic geometry for these initial conditions. The particle's diameter is the ratio of the core height to that of the core diameter.

From the results above, the scaled PBR has been designed to have a 30 cm core diameter and 45 cm cylinder height which was dictated by the particle's diameter, 1 cm.

المنارة للاستشارات
www.manaraa.com

Table 3.2: Real Pebble Bed Reactor scale

	HTR-10	HTER M200	PBMR	GE-MPBR	VHTR300	VHTR600	AVR
core D	180	300	350	144.8	300	500	300
core H	197	940	850	926	875	950	280
pebble d	6	6	6	6	6	6	6
D/d	30	50	58.33	24.13	50.00	83.33	50
H/d	32.83	156.67	141.67	154.33	145.83	158.33	46.67
H/D	1.09	3.13	2.43	6.40	2.92	1.90	0.93

The ratio is as follows, 30: 45: 1. This is indicated as (core diameter D/pebble diameter): (core height H/pebble diameter d): (core height/core diameter).

Generation IV reactors (Gen IV) will be developed for the criteria system of the VHTR (Very High Temperature Reactor). Pebble Bed Reactors (PBRs) of a cylindrical vessel with a conical hopper will be implemented in the scale-up properties. This includes the following components: a helium coolant gas to boost the heat transport, graphite-moderator pebbles and fuel pebbles with their mixing recirculation in the reactor system. First of all, the reactor's scale will exhibit normal reactor temperature while adjusting the PBRs geometry (enriched fuel and moderator amounts) and its associated power cycles for determination of the burn-up. We focus on the PBRs ratio of the reactor core diameter/height and the hopper angle in terms of the stresses by a Continuum Mechanics (bulk solid) given by the pebble particle's size. Scale-up supports the following parameters: transient granular dynamics (mass flow rate and packing conditions) and radiation detection-optimization conditions for tracking the pebbles. Secondly, the performance of radioisotope tracking within the scaled reactor in the lab setting will determine the preliminary analysis.

www.manaraa.com

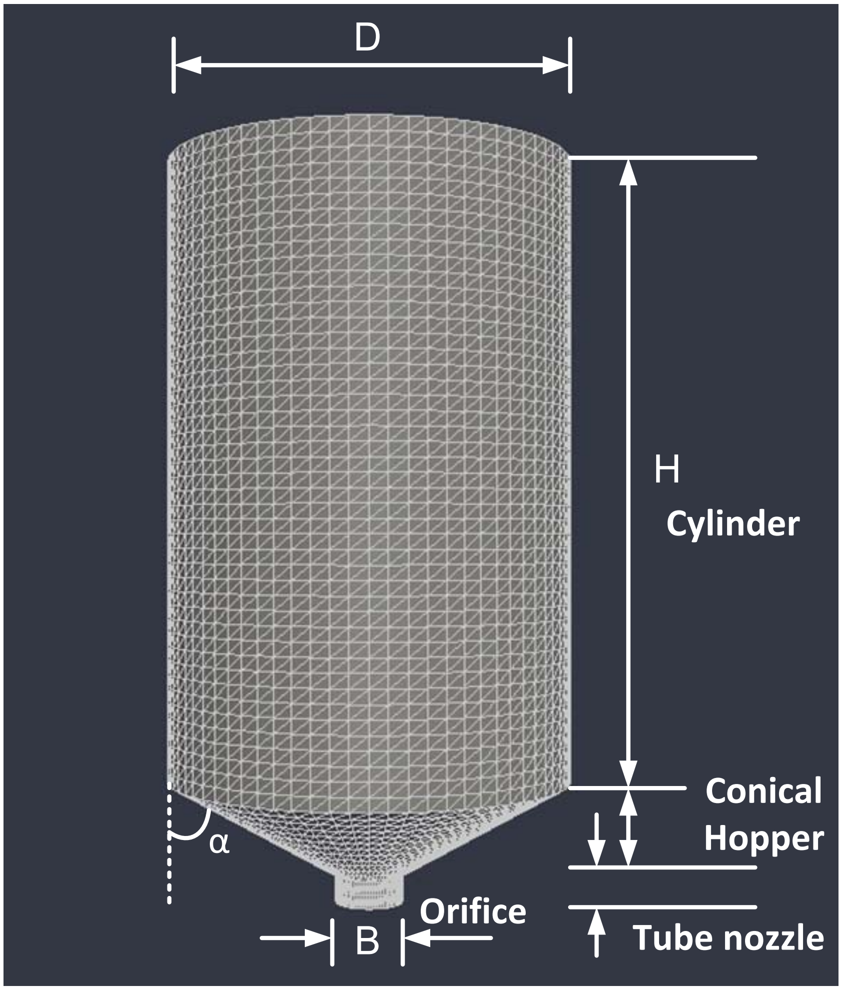

Figure 3.1: Schematic of Pebble Bed Reactor showing vertical cross sections for a cylindrical vessel with a conical hopper

www.manaraa.com

Due to a heterogeneous medium, where there is a random packing condition of pebbles, tracking the pebble as an individual radioisotope particle within the reactor will result in a highly inaccurate result for position detection. A time-dependent mass can be calculated by a regular interval along the reactor height. This is based on the mass flow of the pebbles granular material where the reactor container is included within its associated packing fraction. Effective and maximum scale can be determined using a relative approach with or without pebbles. The approach is based on using LAMMPS/LIGGGHTS to measure the density and their analysis can be obtained from an associated mass flow type prediction. The limitations imposed are the granular mechanical properties characterized as angles of the reactor's geometry in pursuit of the interest of region shape, as in the case of the hopper. Because it is required to identify suitable control of the reactor, this preliminary assessment allows us to make PBRs configurations with the critical scale-up conditions. For the fixed size of the pebble diameter, the optimum design criterion of the scale up is indicated to reduce the factors.

Pebble Bed Reactors are designed as a cylindrical vessel with a conical hopper. The conical geometry has an advantage in the stability of axi-symmetric shape function by passing pebbles through the interior of the reactor under controlled mass flow rates and the residence time. The benchmark of the scaled PBRs is constructed with a 30cm core diameter. The particle diameter is the ratio of the core height to that of the core diameter. As shown in Figure 3.1, the scaled PBRs for this design has been designed to have a 30 cm core diameter (D) and a 45 cm cylinder height (H) which was dictated by the 1cm particle diameter (d). The ratio is as follows, 30: 45: 1.5, which is indicated as (D/d): (H/d): (H/D). The base of the reactor at height z=0 is extended downwards by a vertical tube nozzle of length 2d. The size of the orifice (B) could be adjusted to be different with 3.5d, 5.0d, and 6.5d configurations. The angle of the hopper, α, is placed

المنارة للاستشارات
www.manaraa.com

on the vertical axis of the cylinder connected to the conical wall, which has a slope of 75°, 60°, and 45° respectively. According to the size of the orifice and the angle of the hopper, the boundary mesh of the reactor's wall is enclosed to incorporate the effects of stress in configurations from one end to the other through the granular dynamics. The functionality serving as a three dimensional surface geometry, wall surface mesh, is generated by using a formatted stereolithography (STL) file created with common CAD software. Consequently, it is important that the simulation process is designed and operated with a view to the pebble–wall collision.

All PBRs can be constructed in a scale-up fashion and presented by MD simulation (LAMMPS/LIGGGHTS) with the governing equations of each particle interaction in terms of the pebbles being tracked. The important benefit is to evaluate a new geometric configuration. We will implement the characteristics of pile and discharge in a Pebble Bed Reactor described as a three dimensional granular dynamics system.

3.2 Simulation Setup and Procedure

In simulations, it is desired to estimate the system of the reactor by dynamically varying controls for the mass flow rate, the residence time, and the operating system. In particular, the operating system effectively allows for the circulation of the pebbles. This is accomplished by creating the pile and the discharge in a natural process, either on stationary or dynamic patterns in the reactor. Thus one can characterize the effect of a stationary pattern in the reactor for an extended time or that of a dynamic pattern in fast throughput. The pile mode and the discharge mode are regulated by the core bottom.

The principal role is realistic in RBRs systems. The configurations of the initial

المنارة للاستشارات
www.manaraa.com

conditions and their associated boundary conditions were generated in preliminary trials. Pebbles, which had an initial velocity of 1m/s influenced by gravity, are poured into the reactor as a continuous feed in the defined size of cylinder between z=45d and z=65d with the diameter of 10d packed in the random packing condition (with maximum volume fraction limit, 0.64 and mass flow 0.3 kg/sec). The number of identical particles was 20,000, each with a diameter of 1d and a density of 2500 kg/m^3. The particles flow was blocked at the core bottom of the hopper until the pebbles are settled down. In order to perform a discharge of the pebbles, the mode was obtained from the initial position condition of all pebbles. This was read from the input file after the pile was created from the simulation of the pouring of the pebbles. As soon as the bottom boundary was opened, the type of discharge can be identified by mass flow rate and also be determined by stress analysis on the fixed wall enclosed inside of the mesh. This occurs because the reactor was designed to depend not only on the geometry, but also on the angle of hopper. Finally, in relation to the angle of repose and the orifice size, the transitions can be distinguished and rationalized with the similarity and the difference. This allows us to understand the collective behavior and their effectiveness. Therefore, the crucial discharge condition was determined by an arrangement that occurred between the characteristics and respective flow rates effects. As a result of using the preliminary test for optimization of the efficiency to obtain a stable discharge, specific configurations will be selected and investigated for the analysis concerning these phase transitions in relation to their packing fraction and the coordination number. In addition, the volume is calculated in each geometry (Appendix B)

The simulation parameters were applied to all geometric conditions. Identical particles have similar physical material properties such as Young's Modulus of elasticity, Poisson ratio, and frictions (the particle-particle and the particle-wall type) etc. The

المنارة للاستشارات
www.manaraa.com

parameter settings were the same as used for the three-dimensional system presented in Table 3.3. The time step size used was 1×10^{-6} sec. All data was recorded, including the position, the transitional velocity, the angular velocity, and the force of each particle.

The granular materials are made up of particles that are substantially mono-disperse and are described by the following table of the material properties. The empirical correlation between different materials was employed into both the particle-wall interaction and the particle-particle interaction.

Table 3.3: Physical Properties and Simulation Parameters

Parameter	Symbol	Units
Particle's diameter	d	10 mm
Particle's density	ρ	2500 kg/m^3
Young's Modulus particle-particle	E_{pp}	5×10^8 Pa
Young's Modulus particle-wall	E_{pw}	8×10^9 Pa
Possion ratio particle-particle	ν_{pp}	0.3
Possion ratio particle-wall	ν_{pw}	0.3
Coefficient of Coulomb friction: particle-particle	μ_{pp}	0.5
Coefficient of Coulomb friction: particle-wall	μ_{pw}	0.3
Coefficient of Restitution: particle-particle	e_{pp}	0.35
Coefficient of Restitution: particle-wall	e_{pw}	0.5

المنارة للاستشارات
www.manaraa.com

Chapter 4

Results and Discussion

The characteristics of pile and discharge in Pebble Bed Reactors are investigated to describe the system of three dimensional granular dynamics. Numerical simulations are presented by using Molecular Dynamics through the deformable Hertz's law of the interaction between particles. A pile of pebbles on the top is dependent on mass flow rate with initial velocity 1m/s influenced by gravity in the downward direction. The initial packing fraction of the particles is 0.64 and the number of identical particles is 20,000, each with a radius of 5 mm and a density of 2500 kg/m^3. The initial positions are based on random numbers. Identical particles have physical material properties such as Young's Modulus of elasticity, Poisson ratio, and the coefficient of restitution and friction (the particle-particle and the particle-wall). The particle flow is blocked at the bottom of the funnel. The simulations are monitored continuously and displayed in real time on post processing, using Paraview visualization tool. The parameters, such as the mass flow rate and energy, etc., were calculated from the forces, velocities and positions of each particle for all simulations at different flow regimes and different geometries according to the hopper angle and the orifice ratio. The mass flow rate of the piling and

المنارة للاستشارات
www.manaraa.com

discharge were used to obtain the regression results from the mass-time plot. The piling was performed to pour into reactors under the same conditions of the mass flow 1.6852 kg/sec through circular cross section of diameter 6 cm located at core height 45 cm. The piling and discharge were taken in absence and presence of orifice filter. As the discharge is controlled by the orifice gate after the piling during 20 seconds, then the mass flow rate of the discharge was observed whether or not the flow was obstructed due to jamming in the reactor.

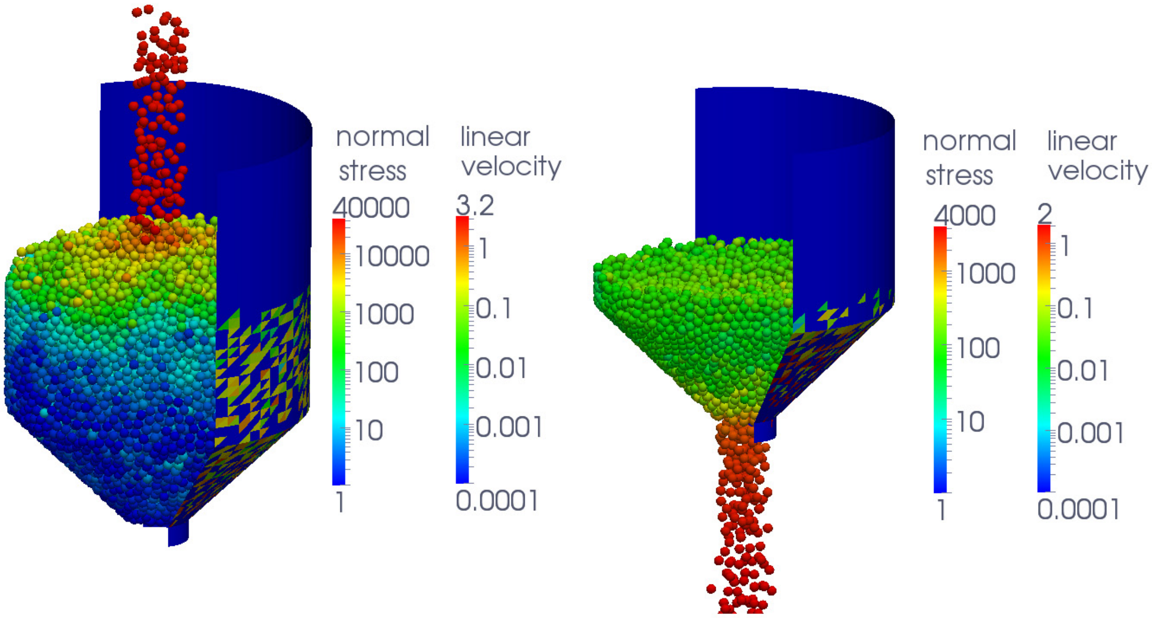

Figure 4.1: Snapshot of piling (left) and discharge (right) with transitional velocity and normal stress given the angle 45° and the orifice size 6.5d

المنارة للاستشارات
www.manaraa.com

4.1 The piling in PBRs

Particles are inserted into the reactor at every time step within an initial region until 20,000 pebbles have been inserted under the influence of gravity at which point the reactor will be filled with particles. The 3D simulation results showed that the pebbles motion is clearly observed in the snapshots according to their instantaneous velocity (transitional and rotational) and the forces of the piling system in Figures 4.2 and 4.3. The piling could be initiated in different types of the reactor to induce the mechanism by which an initial discharge condition is found that situates the coordination number and the volume fraction. The piling may also be characterized as a collection of a random packing condition with spatial-temporal behavior, thus it is used to provide reactor activation for further reactor processes. The mass flow rate plays a key role in the piling which operates with the stress by driven gravity and their collision on the wall and thus forming a normal stress and a shear stress.

The granular dynamics of interacting pebbles in Pebble Bed Reactors has a force chain or contact stress field. In order to analyze the stresses of contact points in inhomogeneous media, the result of network forces should generate normal stress on the wall. Also, the network force part of the Hertz frictional force should produce tangential (shear) stress on the contact wall. The stress behavior of packing pebbles in silos in view of stress and strain is

$$\sigma = \lim_{\delta A \to 0} \frac{\delta F}{\delta A} \tag{4.1}$$

Figure 4.4 shows that σ_n is normal stress and σ_t is shear stress.

www.manaraa.com

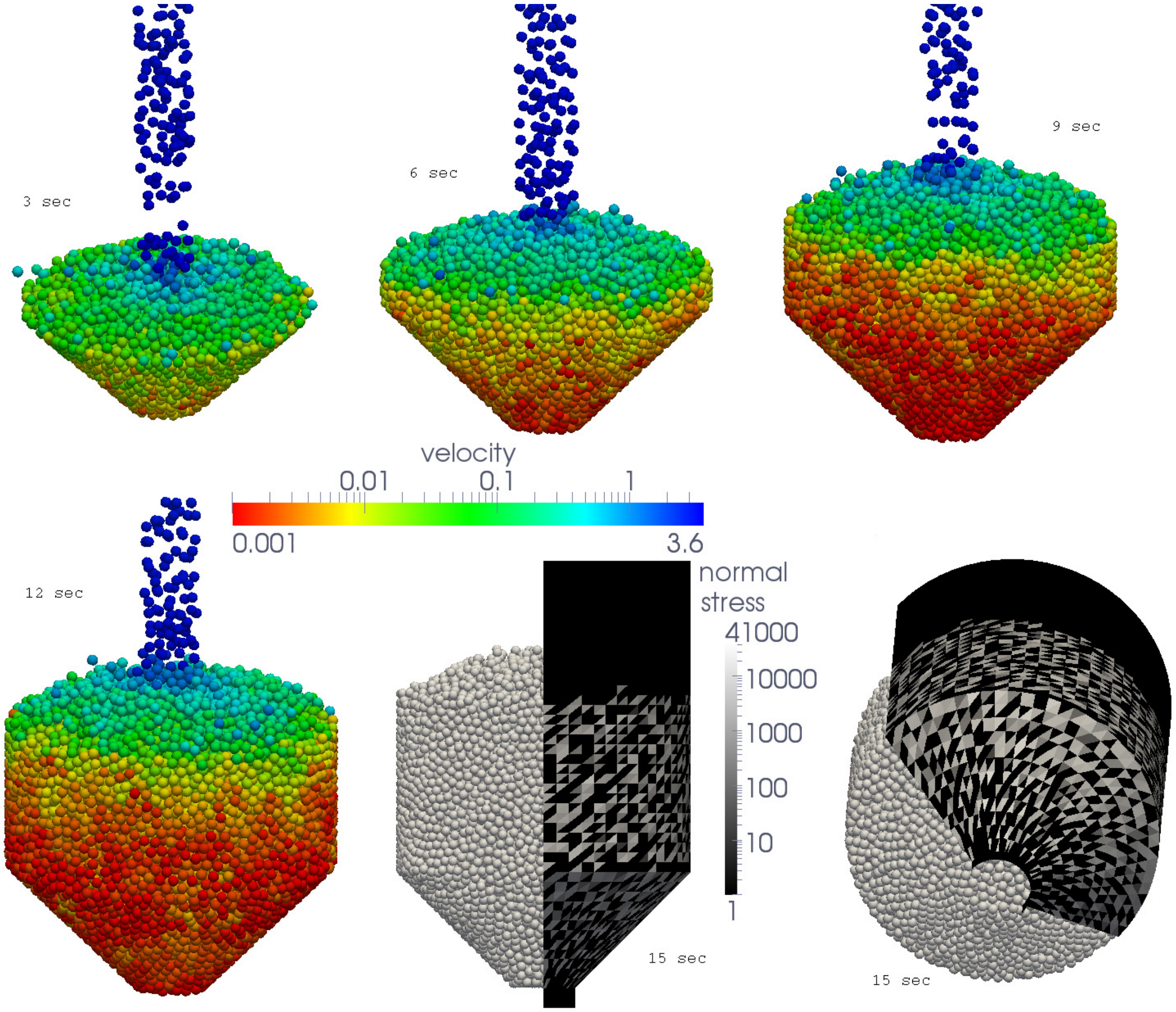

Figure 4.2: Snapshot of piling and stress mesh with linear velocity given the angle 45° and the orifice size 6.5d

www.manaraa.com

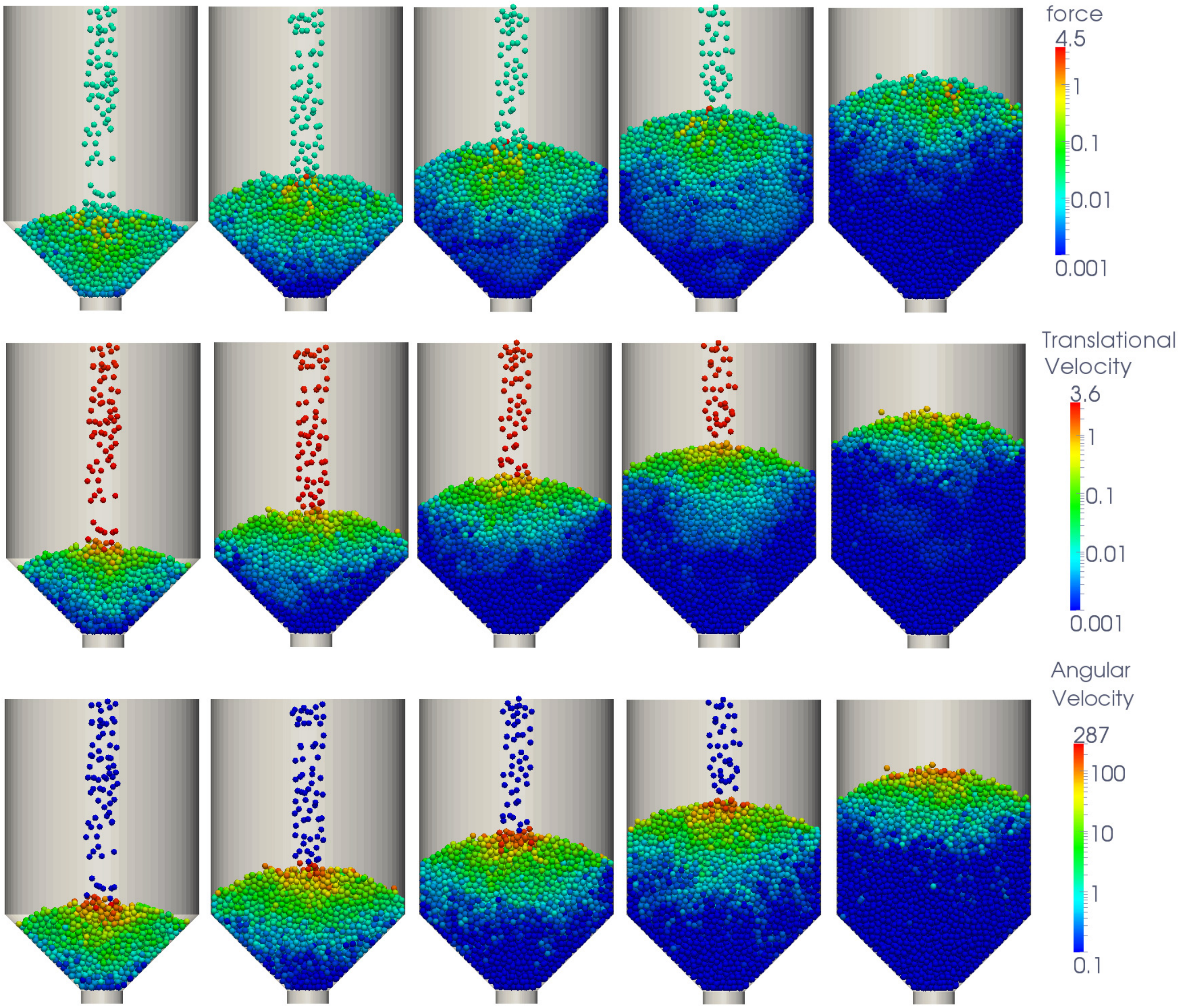

Figure 4.3: Snapshot of force, transitional velocity and angular velocity calculation showing vertical cross sections split in half and top view given the angle 45° and the orifice size 6.5d at times 3, 6, 9, 12, and 15 sec in SI units

المنارة للاستشارات
www.manaraa.com

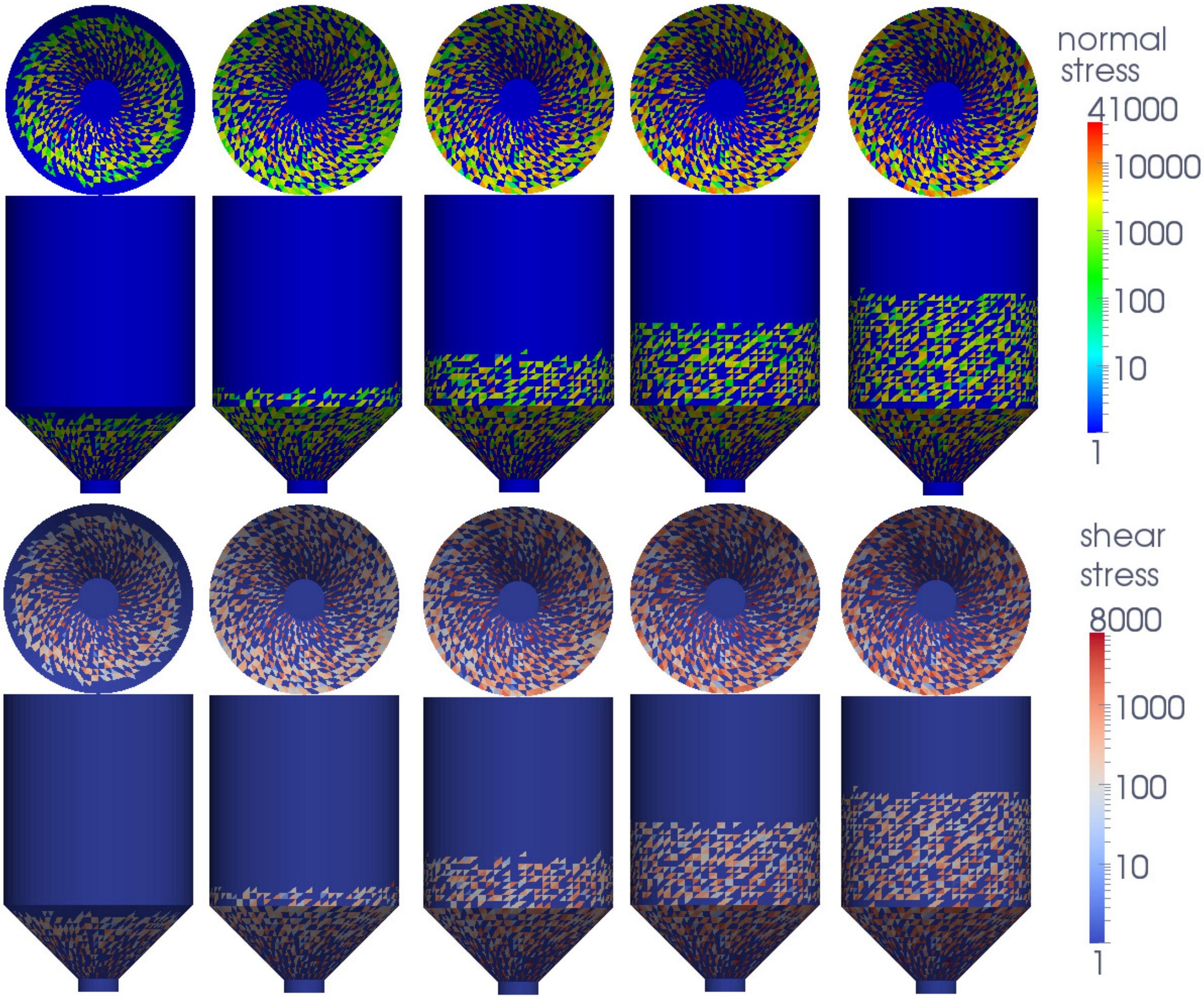

Figure 4.4: Snapshot of normal and shear stress wall given the angle 45° and the orifice size 6.5d at times 3, 6, 9, 12, and 15 sec in unit Pascal

www.manaraa.com

4.1.1 Energy system

The energy system is described from a classical interaction energy. The motion of N monosphere particle in a three-dimensional space is determined by Newton's equation expressed to the total forces and torques. The motion of the ith particle moves along any path in driven gravity force with collisions located at position $\mathbf{r}_i$ with velocity $\mathbf{v}_i$ and angular velocity ω_i

$$\mathbf{f}_i = m_i \frac{d^2\mathbf{r}_i}{dt^2} = \sum_{i \neq j} \mathbf{F}_{ij} + m_i \mathbf{g} \tag{4.2}$$

$$I_i \frac{d\omega_i}{dt} = \sum_{i \neq j} \mathbf{r}_{ij} \times \mathbf{F}_{ij\perp} \tag{4.3}$$

The total kinetic energy of the system, consisting of the sum of the translational kinetic and their rotational kinetic energy with ω_i angular velocity about the origin, are related to Euler's angles, namely,

$$K = \frac{1}{2} \sum_i m_i v_i^2 + \frac{1}{2} \sum_i I_i \omega_i^2 \tag{4.4}$$

The granular temperature is calculated by the mean translational, K_t (Campbell 1990), and the mean rotational, K_r, kinetic energies. The granular temperature is proportional to the mean kinetic energy

$$\begin{aligned} K &= \frac{1}{2} \sum_i m_i v_i^2 + \frac{1}{2} \sum_i I_i \omega_i^2 = \frac{3}{2} N k T \\ \frac{3}{2} k T &= \frac{1}{N} \sum_i \left(\frac{1}{2} m_i v_i^2 + \frac{1}{2} I_i \omega_i^2 \right) = \left\langle \frac{1}{2} m_i v_i^2 \right\rangle + \left\langle \frac{1}{2} I_i \omega_i^2 \right\rangle \end{aligned} \tag{4.5}$$

www.manaraa.com

The total gravitational potential is $V = \sum_i m_i g z_i$, and the total pairwise interaction potential of an N particle system interacting through a pair potential for Hertz-Mindlin contact can be written as

$$\Phi = \sum_i \sum_{j>i} U_{ij} = \frac{1}{2} \sum_i \sum_{j \neq i} U_{ij} \tag{4.6}$$

The virial theorem predicts the interaction potential energy is the sum of the pair force on each particle,

$$\Sigma = \frac{1}{2} \sum_i \sum_{j \neq i} \mathbf{r}_{ij} \cdot \mathbf{F}_{ij} \tag{4.7}$$

where $\mathbf{F}_{ij}$ is the total force acting as part of the MD simulation, and the virial (the pair wise potential) can be calculated. The virial theorem states the expectation value of the sum of the products of the particles and the forces due to interactions between them. In other words, the force moment tensor is characterized by mechanical equilibrium (Ball, Blumenfeld 2002).

Here, the granular stress energy tensor Ξ is defined by

$$\begin{aligned} \Xi &= \sum_i \frac{1}{2} m_i v_i^2 + \sum_i \frac{1}{2} I_i \omega_i^2 + \frac{1}{2} \sum_i \sum_{j \neq i} \mathbf{r}_{ij} \cdot \mathbf{F}_{ij} \\ &= \sum_i \left(\frac{1}{2} m_i v_i^2 + \frac{1}{2} I_i \omega_i^2 + \sum_{j \neq i} \mathbf{r}_{ij} \cdot \mathbf{F}_{ij} \right) \end{aligned} \tag{4.8}$$

where $\sum_{j \neq i} \mathbf{r}_{ij} \cdot \mathbf{F}_{ij} = \tilde{\sigma}_i$ is the contact stress energy term of each particle and $\frac{1}{2} m_i v_i^2 = K_t$ is the kinetic energy of each particle. The granular energy stress tensor is expressed as the internal energy of the system. The mean gradualar energy stress is $\langle \Xi \rangle$.

المنارة للاستشارات
www.manaraa.com

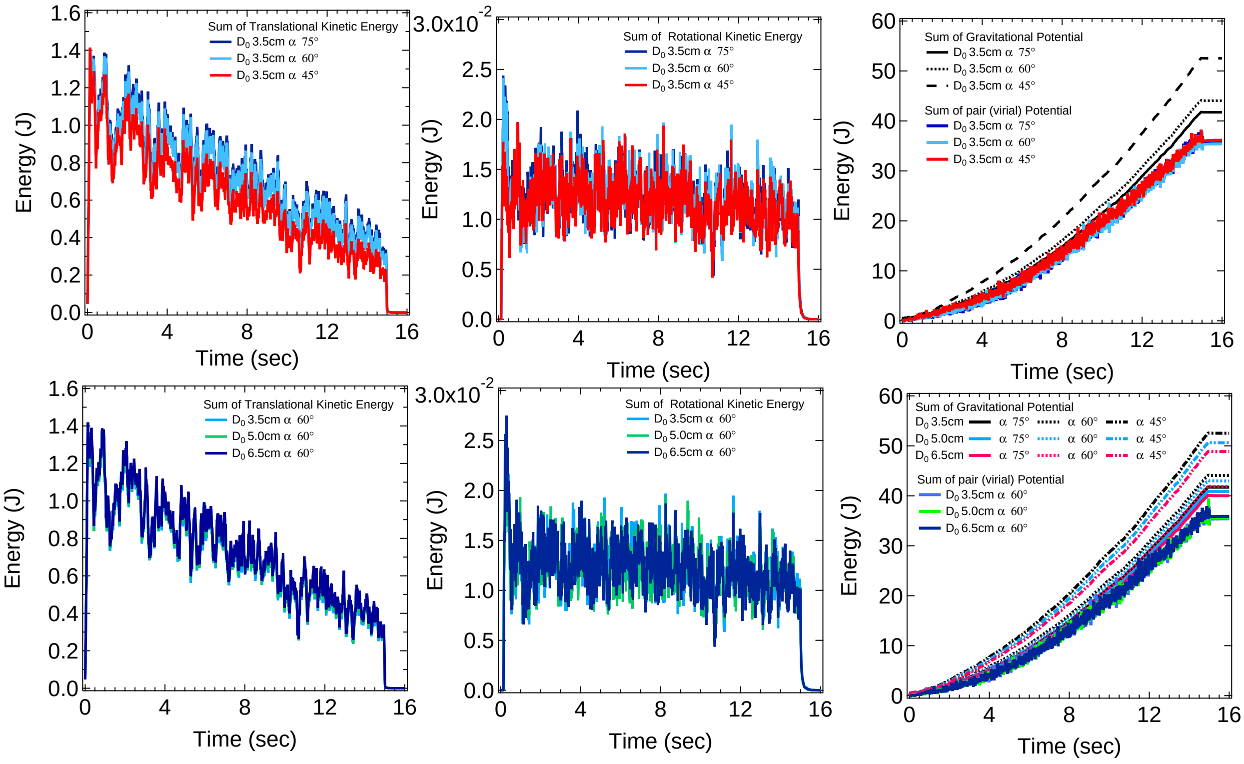

Figure 4.5: Plot of the sum of kinetic energy (translational and rotational) and the pairwise potential (virial) and the gravitational potential as a function of time

المنارة للاستشارات
www.manaraa.com

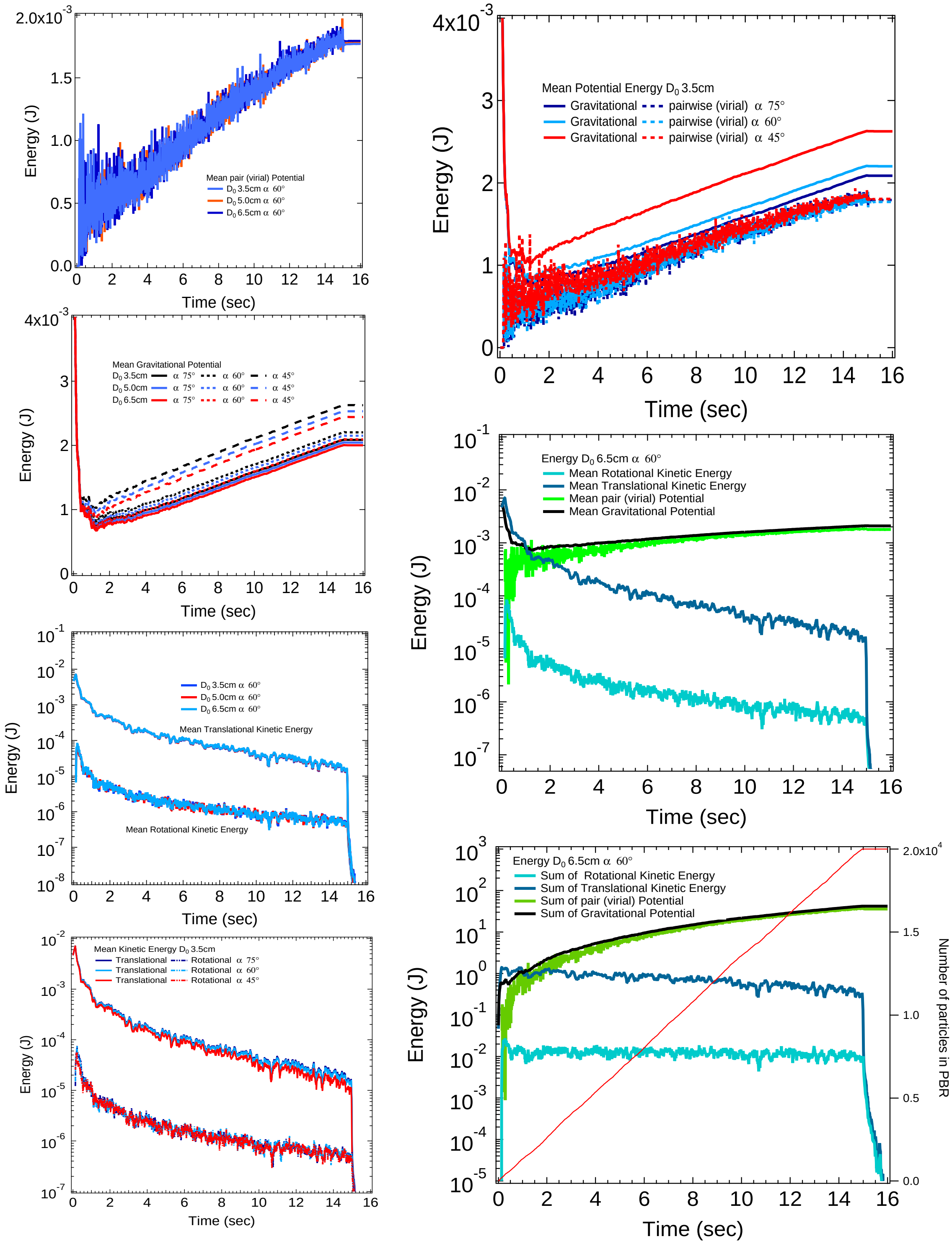

Figure 4.6: Plot of the mean kinetic energy (translational and rotational) and the pairwise potential (virial) and the mean gravitational potential comparing with all energy: mean; sum

المنارة للاستشارات
www.manaraa.com

Pebbles falling into the vessel are initially at a height of 45d with a velocity of 1m/sec (z direction) above the bottom of the vessel, as shown in the Figure 4.3. At t=0 sec, the pebble is released by regulating the constant mass flow rate of the particles produced. The discharge orifice is blocked until 20,000 particles are deposited in the reactor. The kinetic energy is composed of two parts as the sum of its translational and rotational kinetic energies. Its kinetic energy is supplied entirely by the gravitational potential energy which changes as the vessel is filled. The ratio of the translational to the rotational kinetic energy has a difference of about 1%. The effective granular temperature is correlated with the kinetic energy. For the energy of a macroscopic system, when the number of particles, denoted by N, is increased on time dependence, the kinetic energy in the system of the container is found to be inversely proportional to time through the energy that is dissipated by the coefficient of friction and restitution between the pebbles in the presence of particle-wall interactions. In contrast, the gravitational potential and the force moment tensor are proportional to time. During this piling, as the stack of particles is gradually filled with other particles, the movable distance between the initial birth of the particle and its interaction with the filed pile becomes smaller. The different geometry of the reactor affects this change as the energy behavior dissipated in time. There is a slight change of the translational kinetic energy as a function of the hopper angle. However, the variable of the hopper angle and the orifice size shows no appreciable difference in the rotational kinetic energy. The gravitational potential is dependent on a function of the orifice diameter and hopper angles. The pairwise (virial) potential has different patterns depending on the hopper angle. This angle leads to a difference in the height of particles in the hopper. The result of granular stress energy tensor shows reasonable agreement with a variable of the height z above the bottom, similar to the gravitational potential as shown in the Figures 4.5 and 4.6.

المنارة للاستشارات
www.manaraa.com

4.1.2 Mass flow in piling

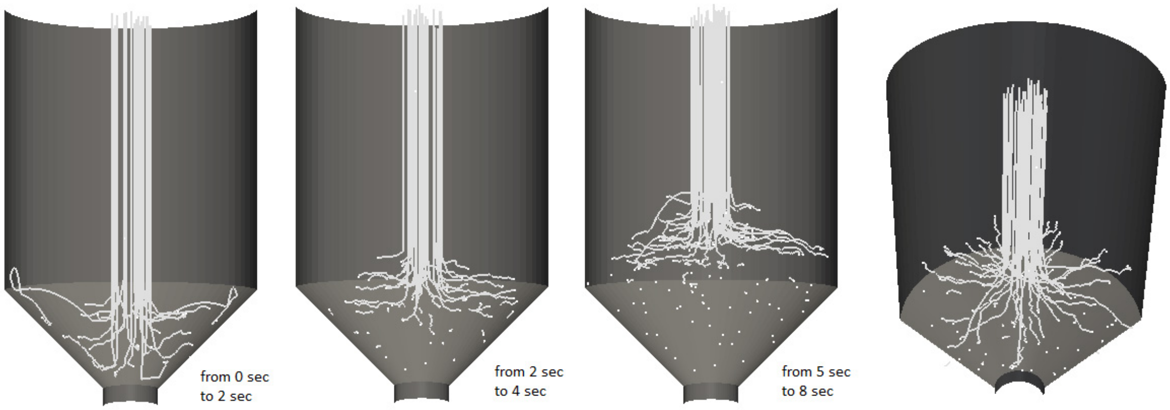

Figure 4.7: The trajectories of particles for tracking in piling case from MD simulation with the hopper angle 45° and the orifice 6.5d under the influence of gravity

The trajectories of selected particles have been explored by MD simulations. The proper time that elapsed between the space-time points depends on the trajectory of each particle. This trajectory of the particles obtained by MD simulations can successfully validate the experiments of the radioisotope tracer. For insight into the dispersed particle behavior to reduce ambiguities, there are spreads in the particle distributions due to collisions after the deposited straight lines as shown in Figure 4.7. The particle tracking appears to be a biased random walk. The parameter of Mean Squared Displacement (MSD) can make the comparison between the MD simulations and the random walks. Trajectories of the particles result in two distinct regions, namely static and dynamic, with a dependence on the external pouring conditions and the wall boundary. The particle tracking method is an easy way to understand the interpretation of the statistical

www.manaraa.com

mechanics.

To evaluate the bulk system, the motion of all particles is calculated using the distance and velocity of center of mass. Macroscopic motion predicts the mean location and momentum of all the mass at time t in the reactor presented as in Figure 4.8. The radius of gyration is used to describe the distribution of the particles or cluster to be concentrated far from the distance from the center of mass. The radius of gyration can be used to infer the phase transitions. The distance of the center of mass shows the correspondence with the gravitational potential until it is sufficient to maintain a stable position at 20 sec. The velocity of center of mass has no effect on the geometry of the hopper angle and the orifice size.

From the transport phenomena, the mass transport can be examined. Figure 4.9 shows the vertical local interval of PBRs piling along with every 3d from the bottom. The core diameter at intervals of 6d expands to the full reactor diameter, 30d in Figure 4.9. Mass flow rates in reactor systems are commonly determined by measuring the flow regime. Specific region flow patterns can be used to analyze the complexity of granular flows in order to find the significant analogies that are valid over the whole system. To identify these flow rate is typified the domain of the residence time monitored a function of the local region and the local core. From the calculations of the mass flow rate in figure 4.9, it is clear that the local mass with comparing with geometry conditions shows the response of a time delay of the capacity. The local mass amounts are proportional to increases due to the local volume. As the characterization of a bulk flow given the local mass flow rate, the first interval region of hopper is occupied by pouring the particles, and then continuously, the second interval region is filled by the particle according to the total mass flow of the system subjected to steady-state. The total mass flow is equal to the sum of local mass fragments of the cumulative probability distribution of local

المنارة للاستشارات
www.manaraa.com

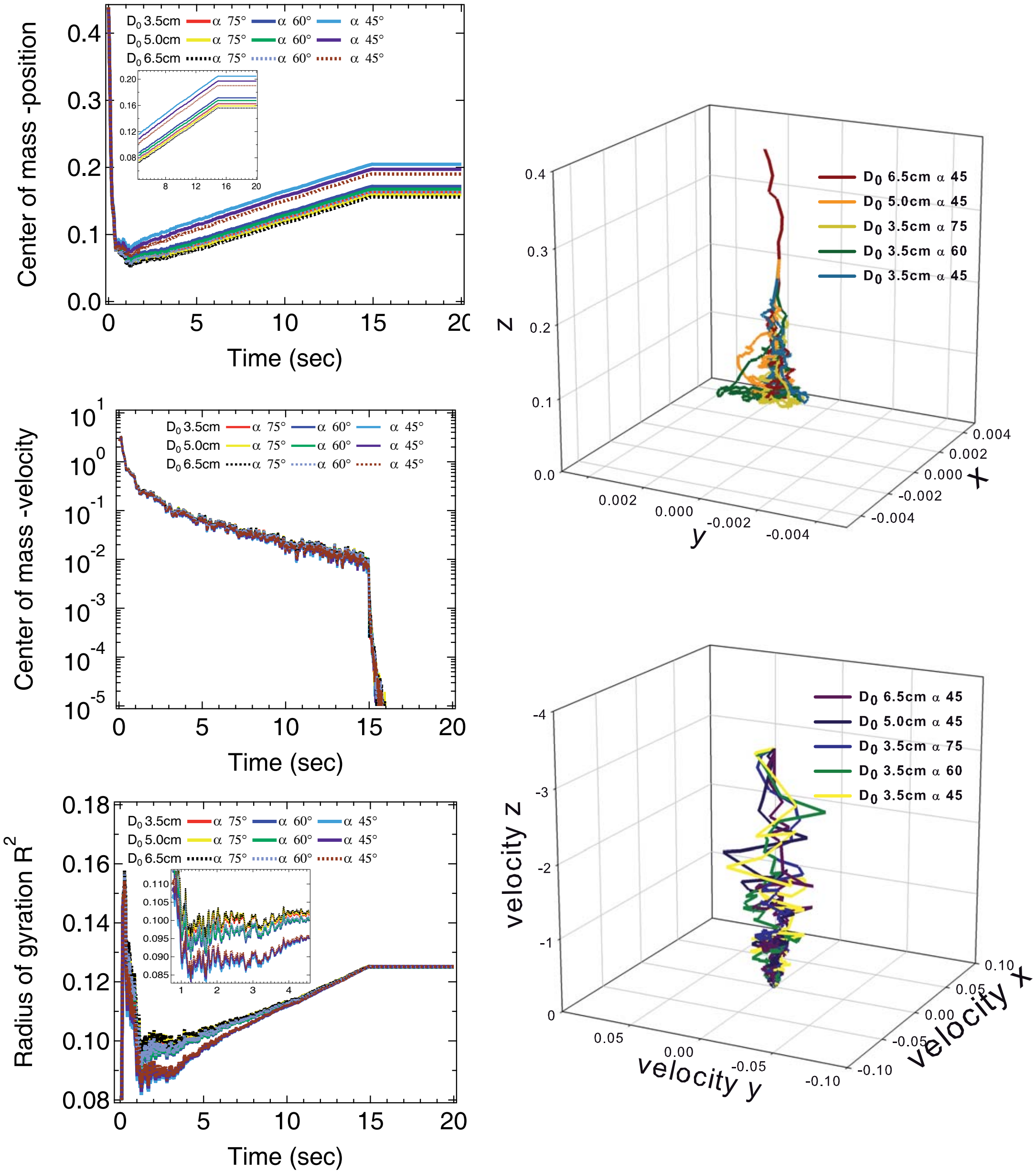

Figure 4.8: Plot of center of mass (distance and velocity), the radius of gyration, trajectory of the center of mass, and the center of velocity presented at each space-time point

www.manaraa.com

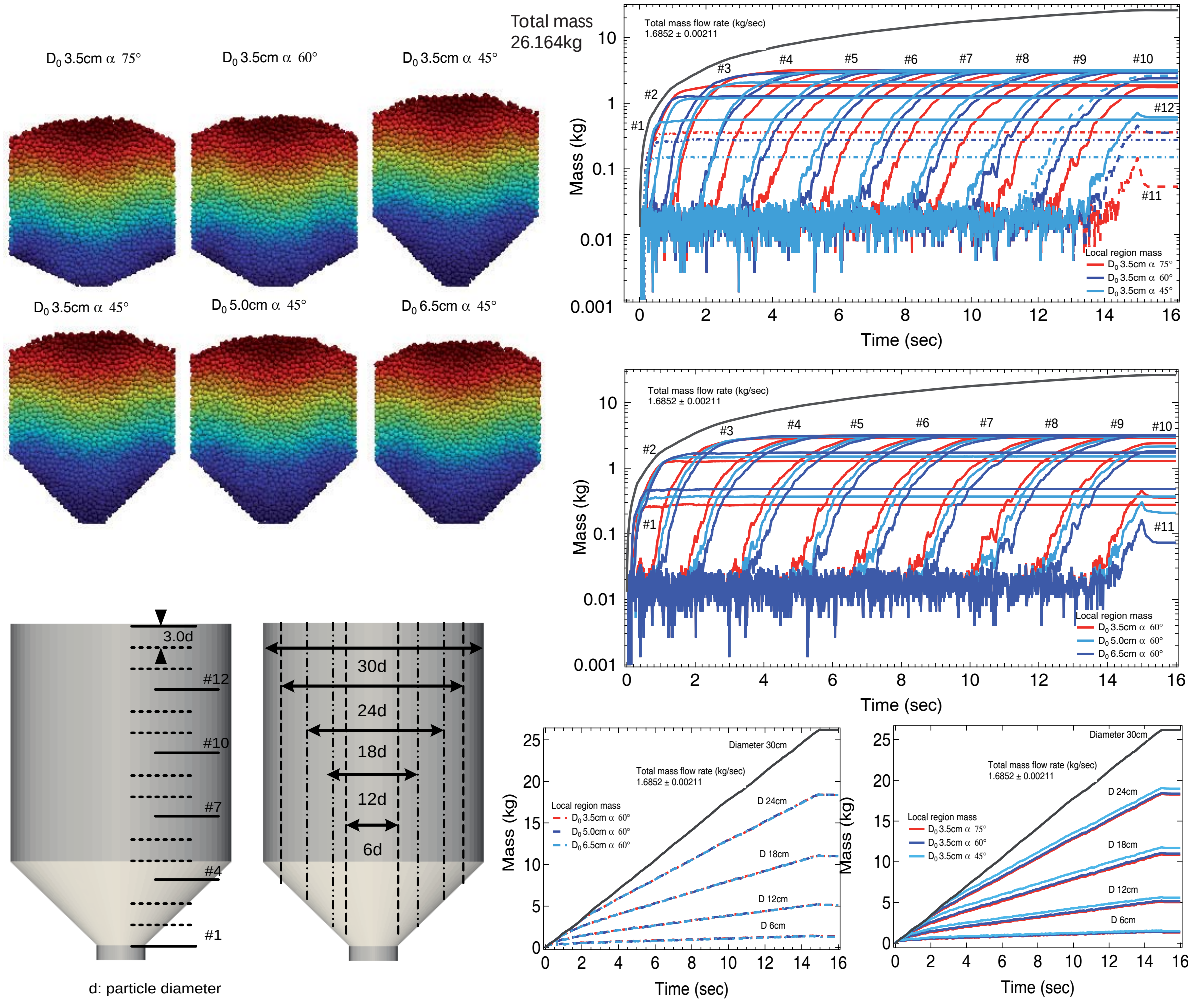

Figure 4.9: Schematic of final particle configurations at 20 seconds and plots of mass flow rate of interval height and increased radius showing vertical cross sections in each local region

www.manaraa.com

mass flow. The correlation to the change in the number (or mass) density and volume (or void) fraction, these changes show that the particle motion fluctuation is indicated by collision effects previously shown in energy calculation results as a function of the dissipation in the pile. However, this is difficult to clarify that the compacting pebble's state is affected by the gravitational stress along the height of the reactor. According to the hopper design, the piling has a difference of the static angle of response and the top of the pile. The mass of the top region is directly indicated by the plot of mass flow rate (the region #11, #12) by fixing the total number of particles, 20,000.

4.1.3 The volume fraction and the coordinate number

The configuration of the volume fraction and the coordination number divides the whole system into local regions which are described by the state quantities. In term of parameters using HertzMindlin theory, the volume fraction changes result from the friction, and the coordination number is associated with the stress within the confines of the regions on mechanical equilibrium. As the pouring particles are filled with the blocked bottom, the coordination number expects an increase in the regime. Although each local volume is held constant, the number of pebbles would remain almost unchanged in the limited volume fraction which is incoming particle takes place. The local volume fraction has the range of RLP (Random Loose Packing) in term of the compactivity of the piling. The static condition at 20 sec is approached at the critical volume fraction (max RLP) with the coordination number, which is calculated by the dependence of the local regime as described in Figure 4.9 (left side). The RLP range on time evolution is identified by our results between 0.54 and 0.60 (Scott ,1960; Onoda and Liniger, 1990). Due to an increase of the stress, the vertical local region is reached to the critical coordination number while the volume fraction of it remains at max RLP. Here, we predict the phase transition

المنارة للاستشارات
www.manaraa.com

of local regions. For frictional spheres, the saturation line corresponds to the critical coordination number, z= 4 in the piling (Silbert, Ertas, et al. 2002). Figure 4.9 (right side) shows that the differences in the local regions (#1, #2, and #3) are affected by the conical volume shape, not the cylindrical shape. The growth rate of the phase diagram has two types of shape functions which are associated with the data points between the linear constant (cylinder) and the curve (#1, #2, and #3). However, the curve shape is driven by the corresponding volume differences from the bottom to the upper region.

It is of crucial importance that the first local region (#1) should be chosen effectively to exhibit the phase transition of primary interest such like an arching or flowing formation. For a statistical description to be reasonable, the qualitative plot of the transition region is shown in Figure 4.11. The infinitely sharp line from $z = 2$ is dominated on left side of the plot, which should be treated as the phase transition. The reason is that the volume fraction on time has peaks. But as shown by on right side in figure, the slanted lines indicate the regime as shown by the curves in figure 4.11. The difference might be attributed to the arrangement which is determined to a flowing or a jamming before the discharge. This result agrees with the jamming on the left of the plot and the unjamming on the right of the plot since the discharge is clearly observed.

www.manaraa.com

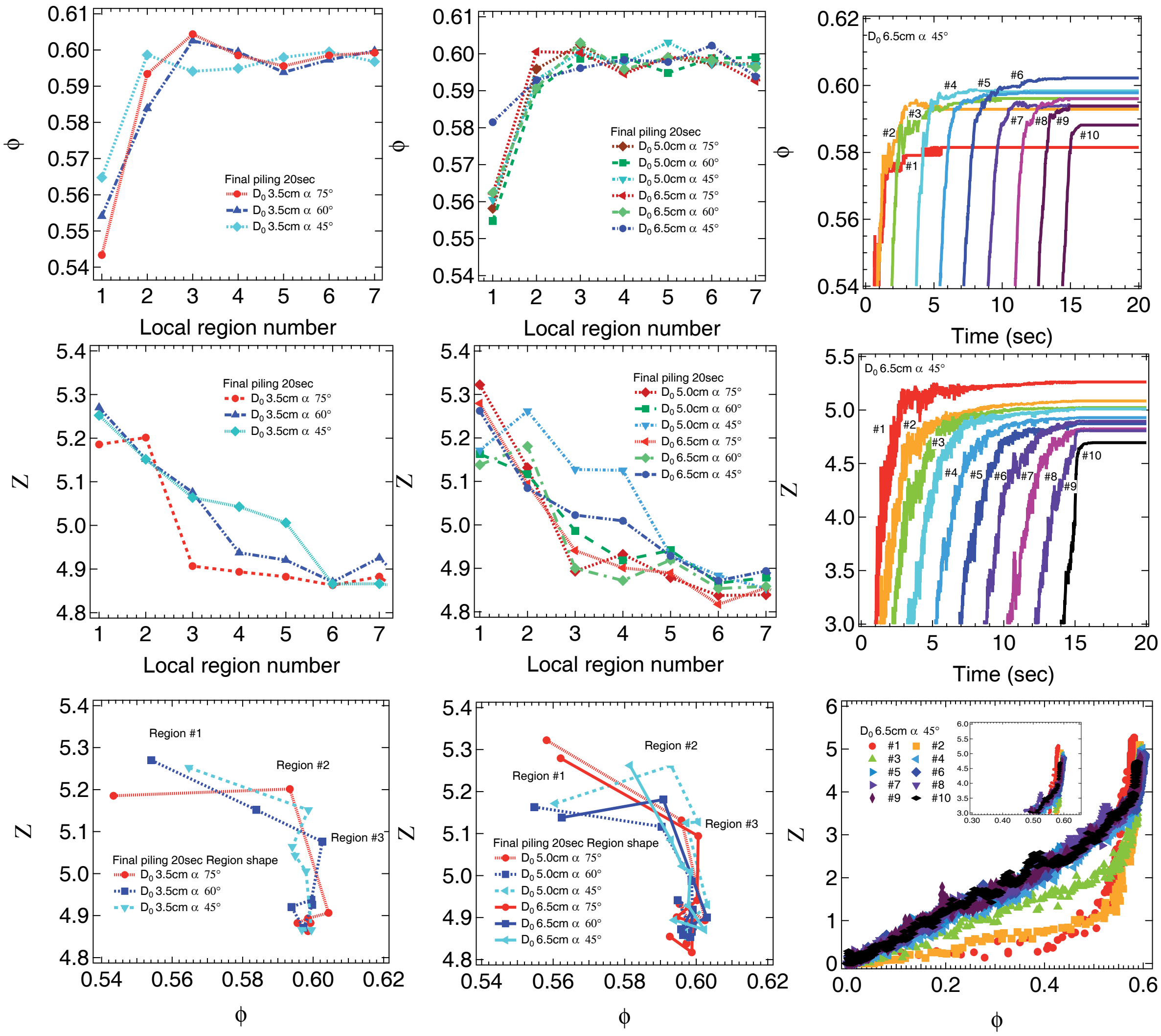

Figure 4.10: Final reached the volume fraction, ϕ and the coordinate number, z at 20 sec (left side) and the domain in relation to ϕ -z (right side) in each region by volume size effect

المنارة للاستشارات
www.manaraa.com

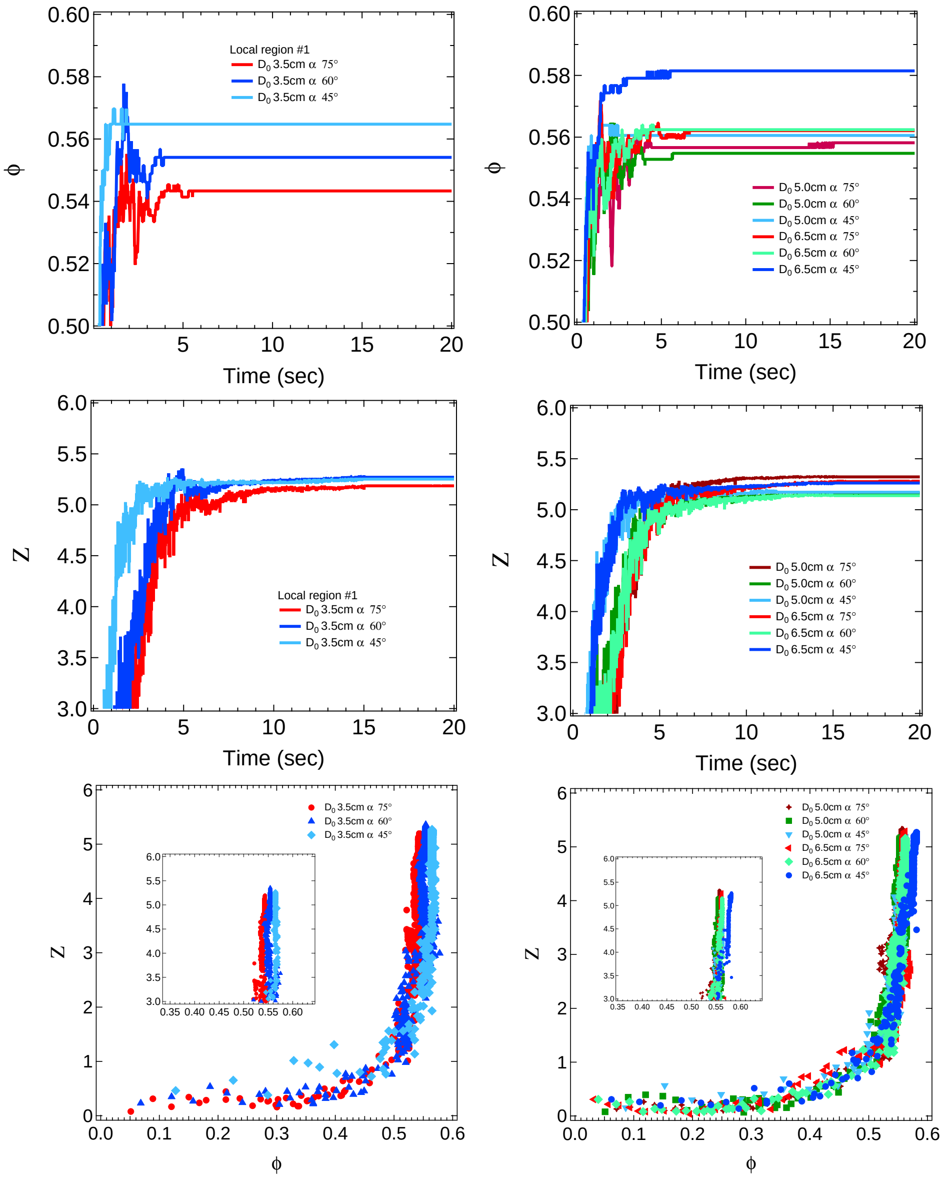

Figure 4.11: Schematic of the volume fraction and the coordinate number on right side in first region between 0 and 3 cm compared with the geometry

www.manaraa.com

4.2 The discharge in PBRs

The discharges have been simulated for the orifice widths (3.5d, 5.0d and 6.5d, where d is the diameter of particle) and the hopper angles (75°, 60°, and 45°). After the reactors were filled with 20,000 particles, the discharge due to gravity is simply operated by the opening of the orifice at 20 sec. This scenario is substantiated by the observed jamming or flowing. The entire orifice of 3.5d exhibited the jamming phenomenon, while others exhibited the flowing with the different value of mass flow rate. The jamming transition in PBRs was examined. A design requirement of PBRs is that no jamming or arching occur (Appendix C).

4.2.1 Jamming

The energy is calculated by the sum of the kinetic energy and the pair potential (virial). The mean energy is obtained from the sum of energy divided by the particles in the reactor. The energy gain peaks have originated from the inner particle motions which are dropped in the reactor as shown in Figure 4.12. The jamming is presented by the volume fraction and the mass flow rate in Figure 4.14. The key point is that the phase diagram of the jamming is presented . The phase line of the volume fraction and the coordination number go down and then the diagonal line is increased. The first local region depicts the previous results in the piling that evaluates this prediction of the jamming transition. The jamming observed in Figure 4.13, the jamming condition by the hopper angle at 75° and the orifice size of 3.5d, is in excellent agreement with the experiment setup. These results demonstrate the remarkable phenomenon related to the rising direction of the jamming transition.

المنارة للاستشارات
www.manaraa.com

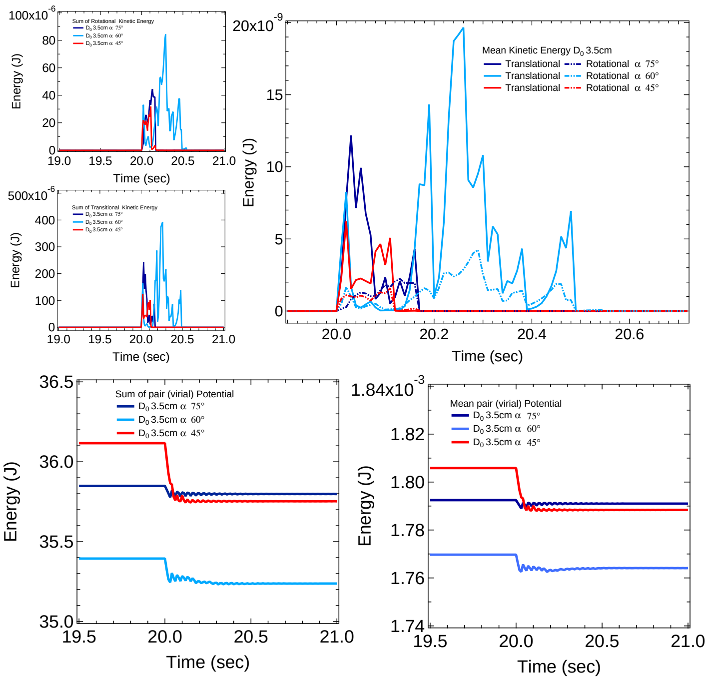

Figure 4.12: Jamming conditions compared with the average and the sum of the kinetic energy (translational velocity and the rotational velocity) and the pair potential (virial) in first region between 0 and 3 cm

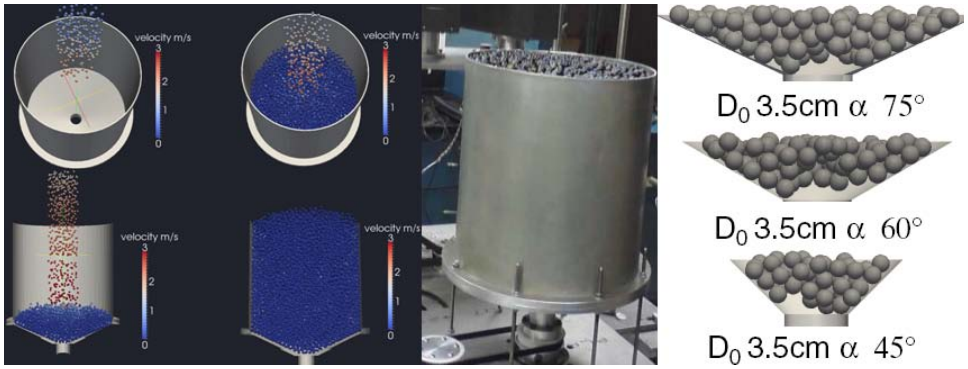

Figure 4.13: Configurations of the experimental geometry (the orifice 3.5 and the hopper angle 75°) with the simulation and the jamming particles in region between 0 and 3 cm

www.manaraa.com

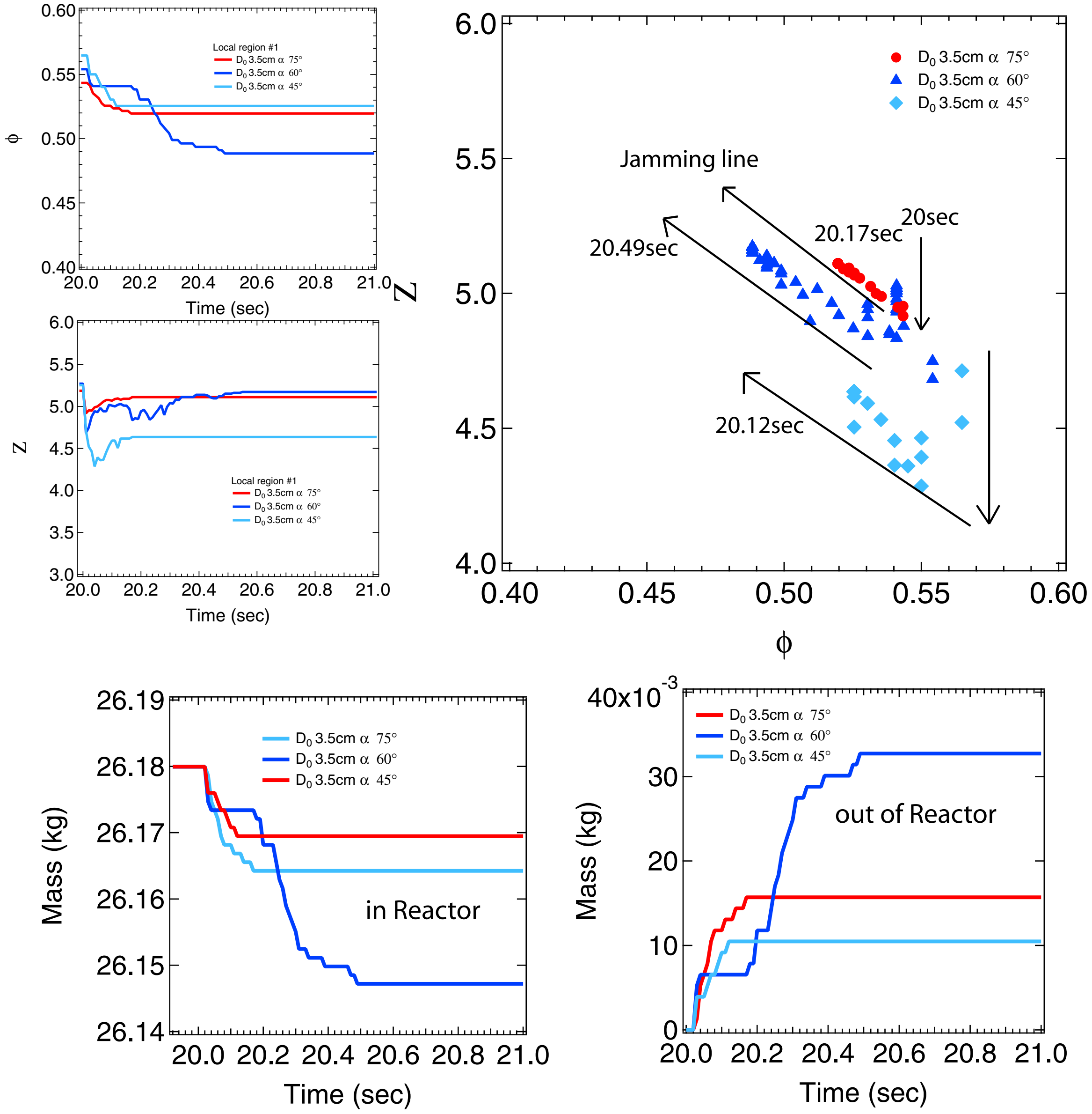

Figure 4.14: Schematic of the volume fraction and the coordinate number outlet mass flow on left side and the volume fraction and the coordinate number on right side in region between 0 and 3cm

www.manaraa.com

4.2.2 Unjamming (flowing)

The flow pattern of PBRs is shown in Figure 4.15. Figure 4.16 illustrates the cross section of the force, the translational velocity, and the angular velocity. The total energy is calculated in Figures 4.17 and 4.18. The computational simulations were performed between 20 sec and 40 sec. However, the 5.0d orifice geometry has not completed the discharge. This gravitational potential is either dissipated with the interactions or converted into the kinetic energy of the flow. The energy in the system is based on the correlation of the mass flow rates. The sum of rotational kinetic energy is about 20% of the sum of translation kinetic energy. These kinetic energy fluctuations could be regarded as the granular temperature effect of the interaction. The mean energy of the system is shown in Figure 4.18. In particular, the mean kinetic energy had a sharp rise and fall by the tail when the particles are almost discharged into the orifice in accordance with the difference in the number of particles.

المنارة للاستشارات
www.manaraa.com

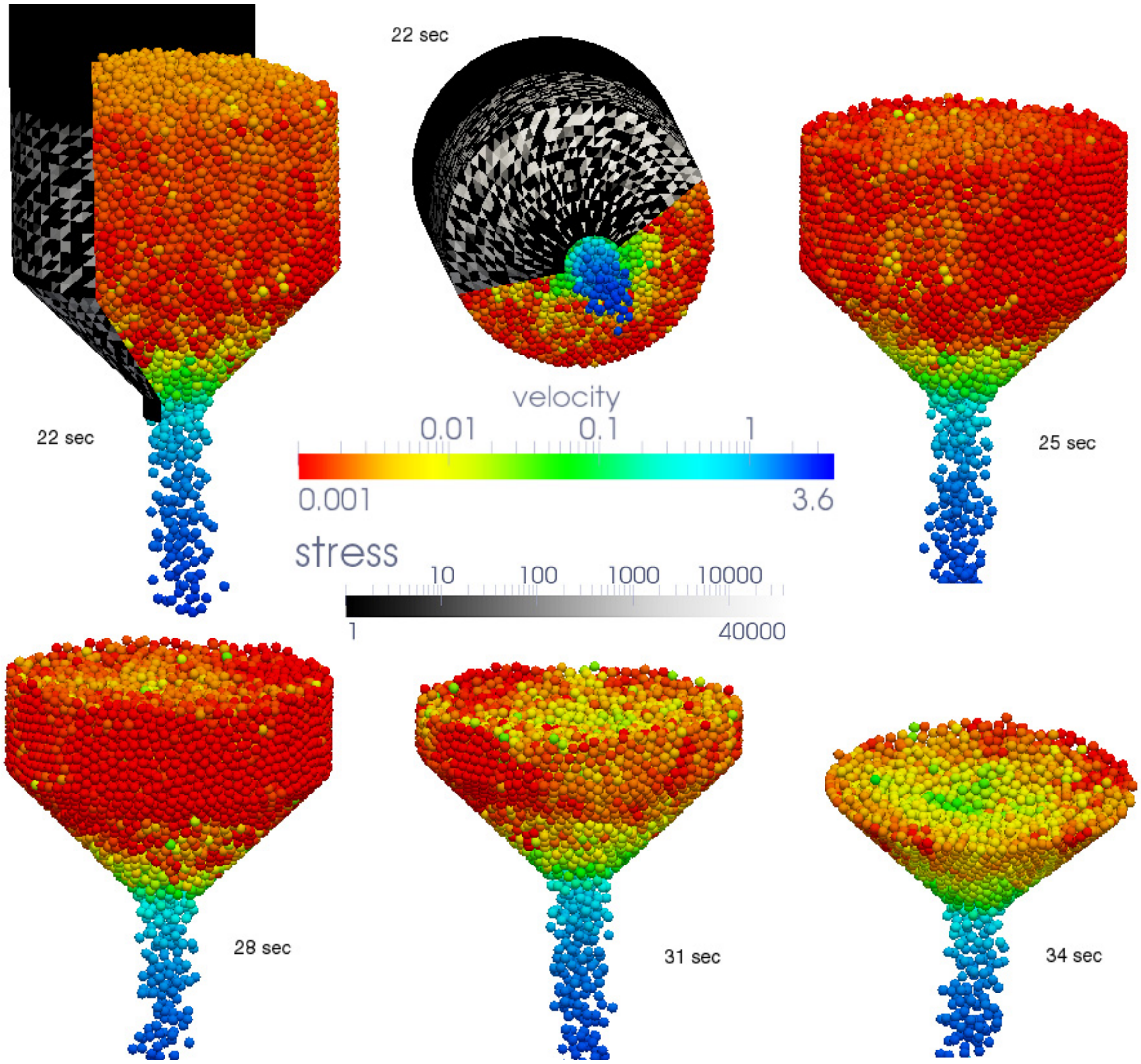

Figure 4.15: Snapshot of flowing and stress mesh with linear velocity given the angle 45° and the orifice size 6.5d

www.manaraa.com

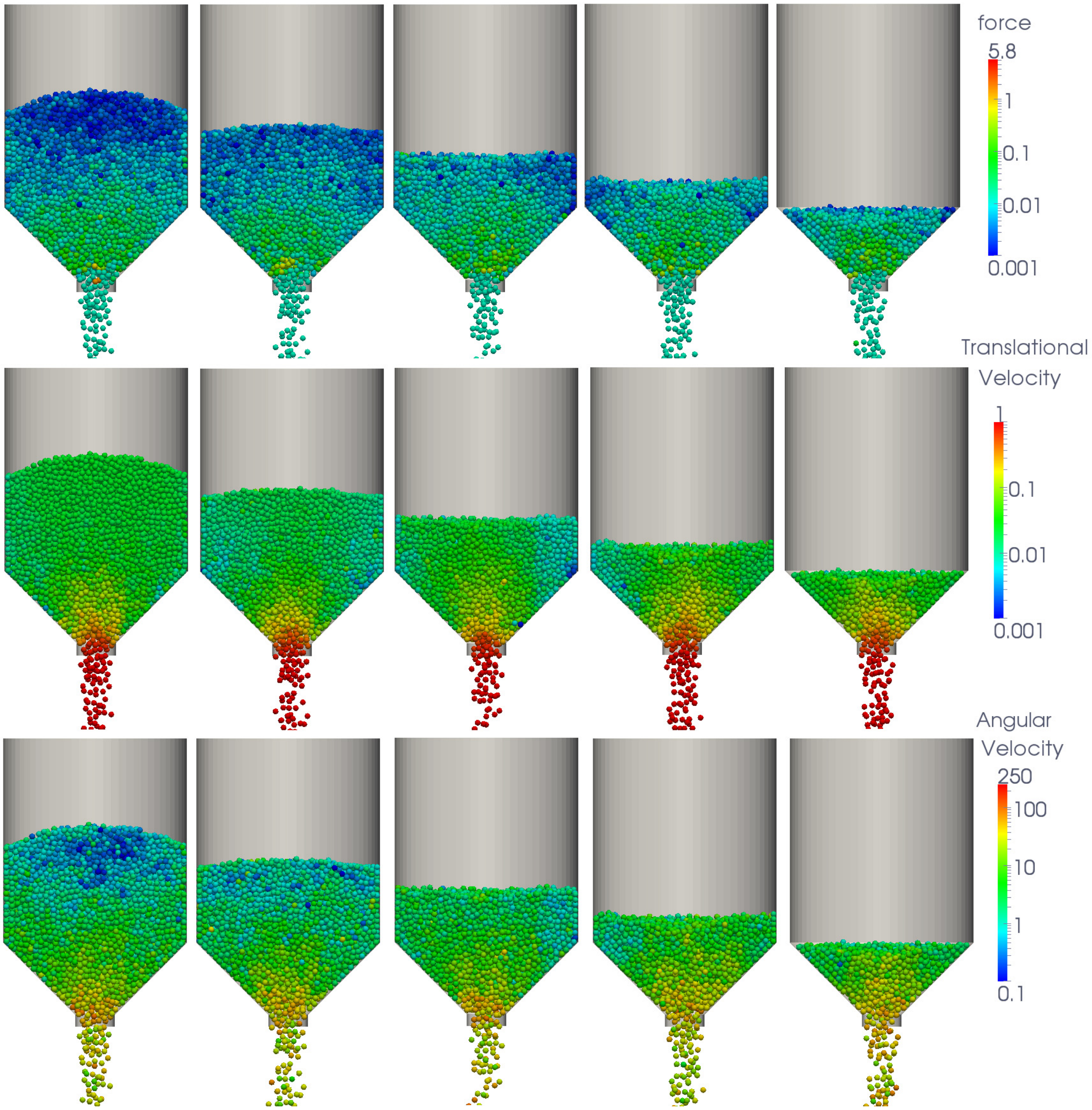

Figure 4.16: Snapshot of force, translational velocity and angular velocity calculation showing vertical cross sections split in half and top view given the angle 45° and the orifice size 6.5d in SI units

www.manaraa.com

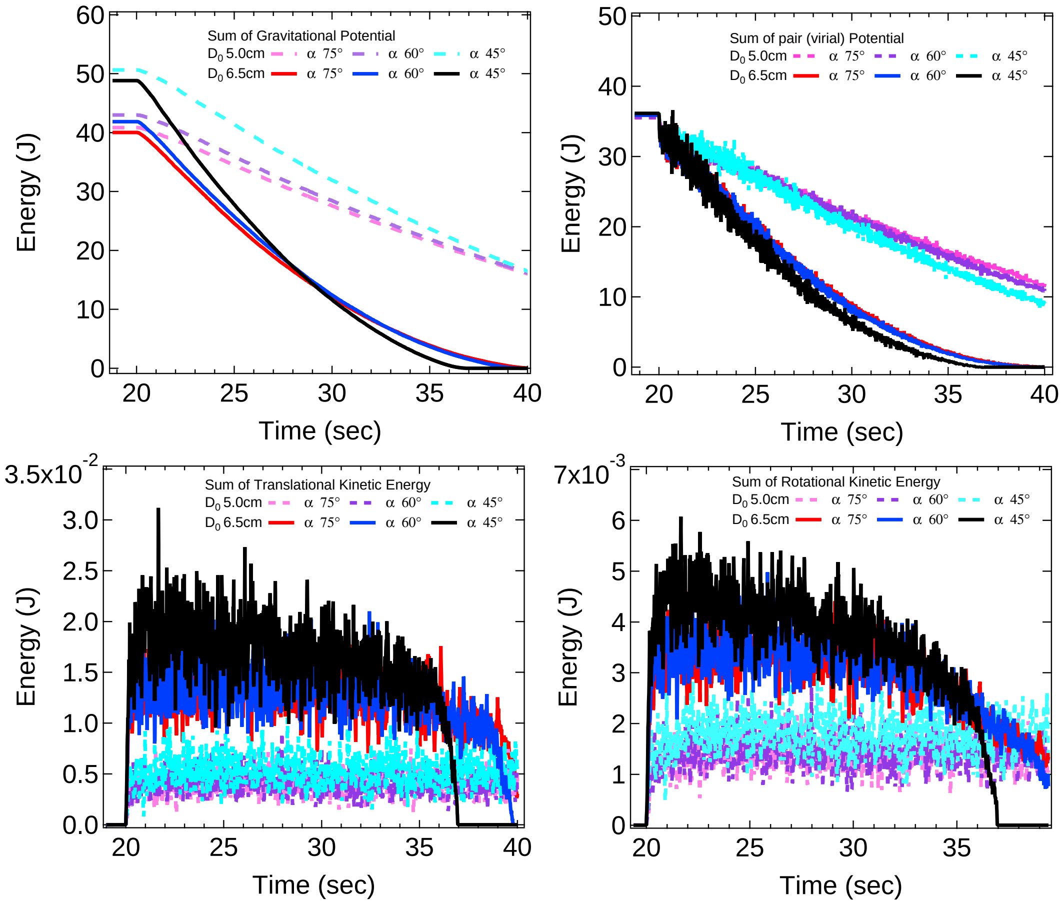

Figure 4.17: For flowing granular Pebbles, plot of the sum of kinetic energy (translational and rotational) and the pairwise potential (virial) and the gravitational potential as a function of time

المنارة للاستشارات
www.manaraa.com

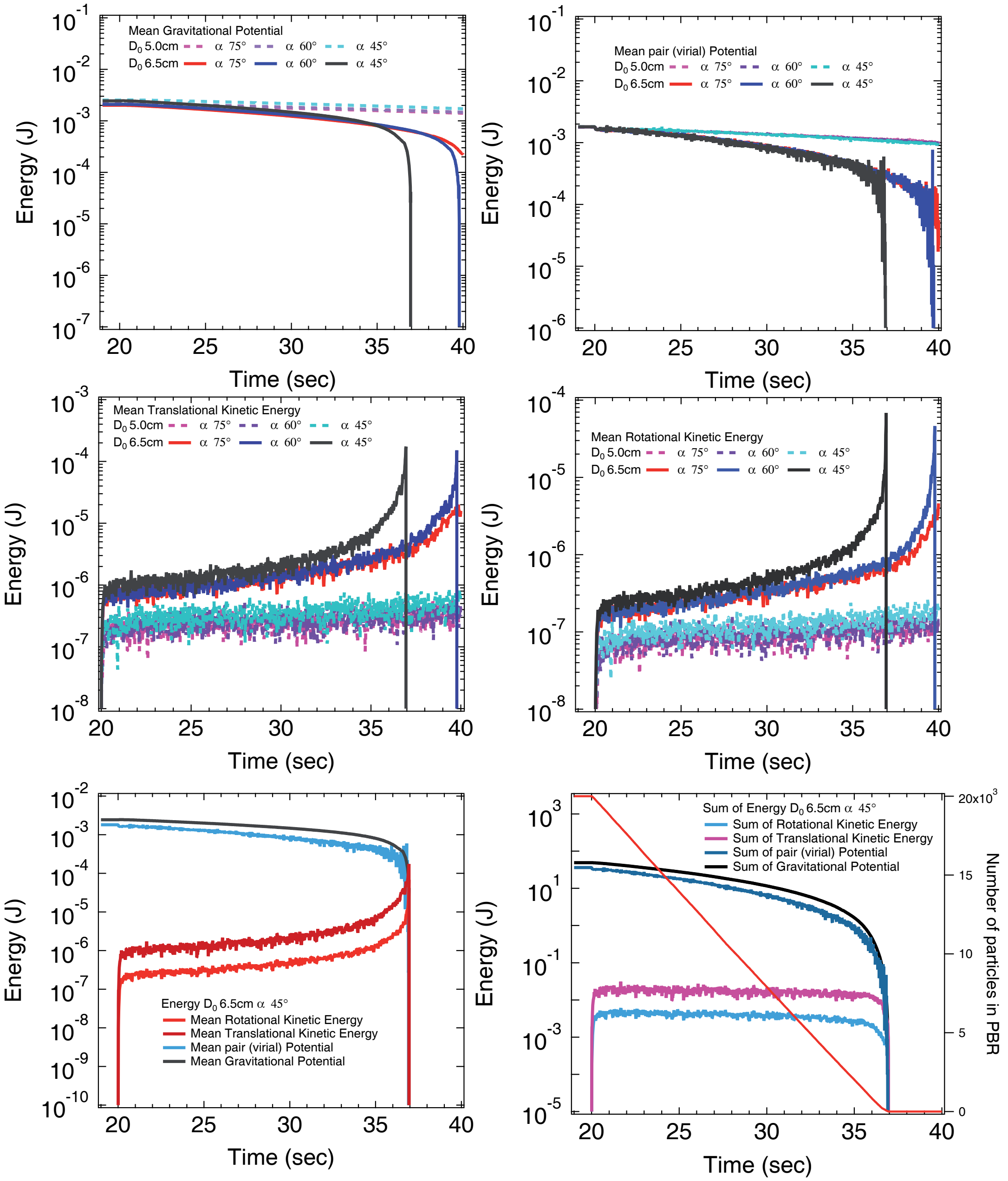

Figure 4.18: Plot of the mean kinetic energy (translational and rotational) and the pairwise potential (virial) and the mean gravitational potential comparing with all energy: mean; sum

المنارة للاستشارات
www.manaraa.com

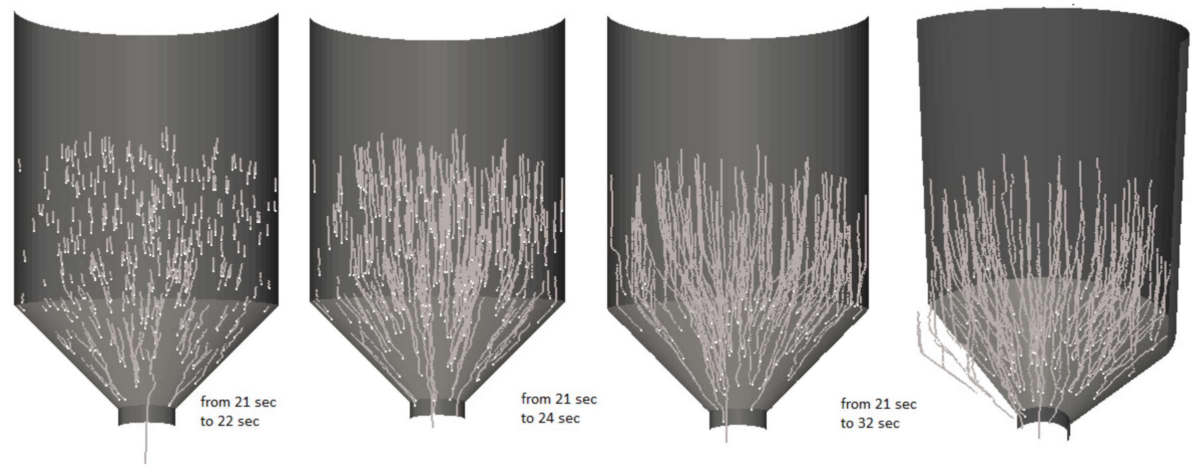

Figure 4.19: The trajectories of particles for tracking in the discharge case from MD simulation with the hopper angle 45° and the orifice 6.5d under the influence of gravity

The trajectories of the flowing particles are presented in Figure 4.19. We can distinguish the flow type by visual observation. The mass flow type has not only steady state flow but also whole particles moving, which is not the stagnation zone in the hopper. The particle position distribution is presented in Figure 4.20. The color scale indicates the order of the particles from 1 to 20,000 particles after the piling. The distribution recessed in the core is affected by the deposited particles on the height 45d. The particle distribution is characterized by the different hopper angles and the orifice widths compared in Figure 4.20. From this viewpoint of the dynamic systems, the snapshot of the distribution in position can be demonstrated for the velocity profile along the heights. The residence time of particles is relevant to the axisymmetric flow. It is eventually shown that the residence time of each particle in the inside corner of the hopper is relatively slower than that in the core due to wall friction and the applied stress.

www.manaraa.com

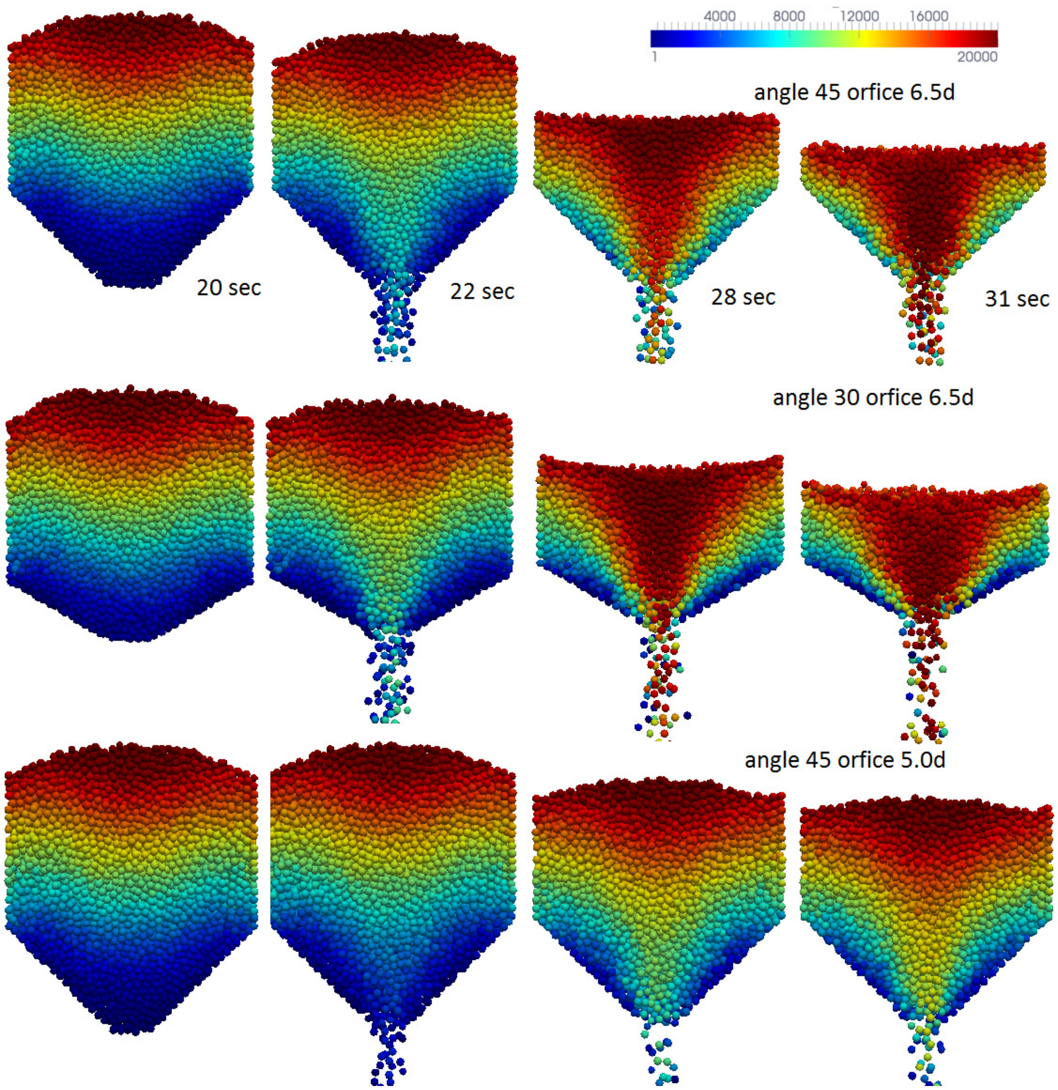

Figure 4.20: Configurations of final particle position distribution at 20 sec and the discharge of the different geometry conditions with the color scale indicating the particle order number

www.manaraa.com

Figure 4.21 shows the distance of the center of mass, the velocity of the center of mass, and the radius of gyration about the hopper angles and the orifice widths with time. As the number of particles decreases with time, the distance of the center of mass is related with the mass flow rate. The velocity of the center of mass represents the average velocity similar to the mean kinetic energy. The radius of gyration describes how far the particles are dispersed from the axis of the distance of the center of mass at time t. The radius of gyration on the time has an unusually sharp convex drop although concave shapes are observed for the gravitational potential, the pair potential (virial), and the distance of the center of mass.

المنارة للاستشارات
www.manaraa.com

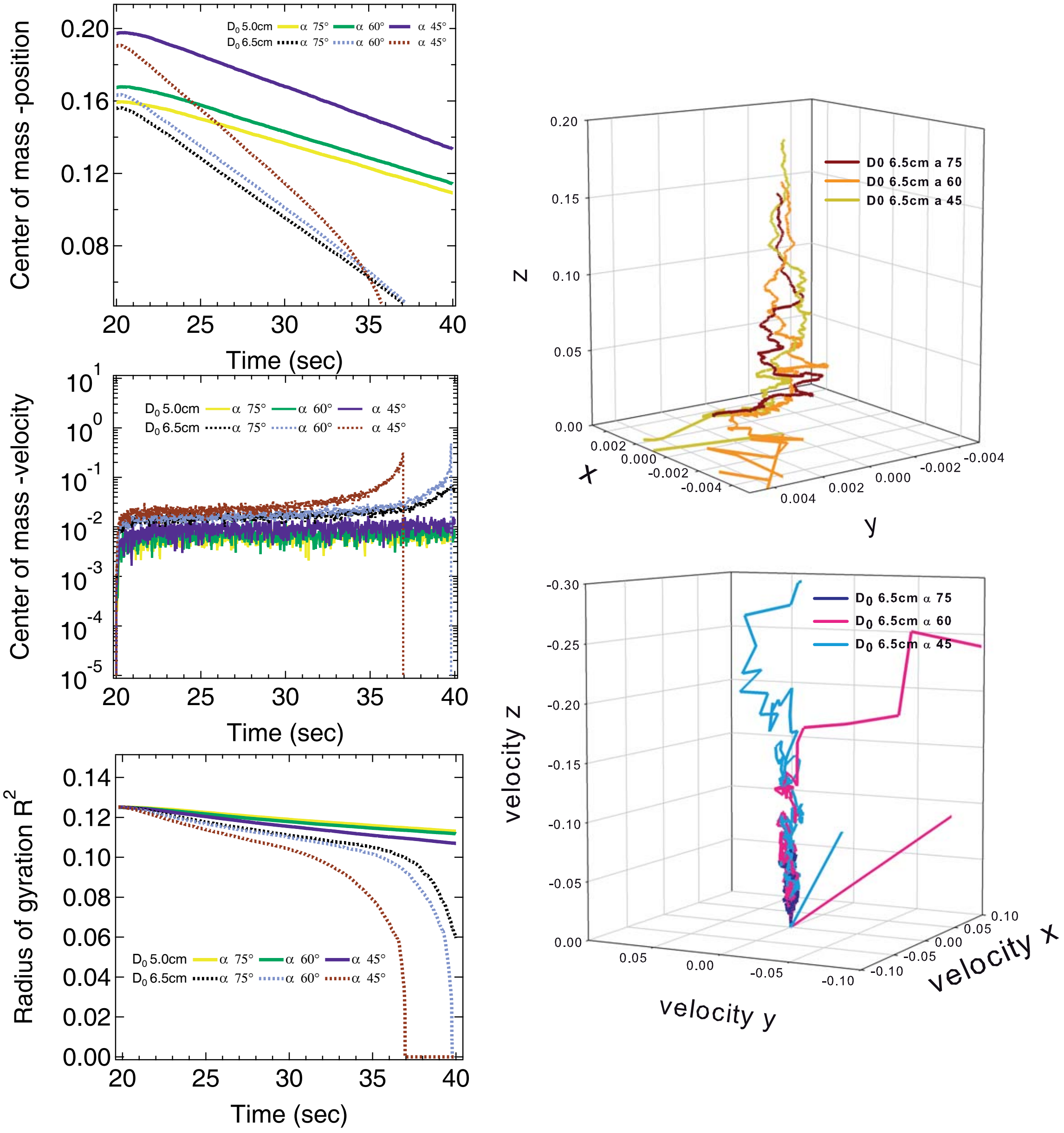

Figure 4.21: For flowing particles, plot of center of mass (distance and velocity), the radius of gyration, the trajectory of the center of mass, and the center of velocity presented at each space-time point

www.manaraa.com

The simulation was carried out with different values of the local volume fraction and the local coordination number when the discharge is generated over the whole system as shown in Figure 4.22 (top). The patterns of ϕ -z were related to the local mass flow rate (bottom-right). The phase diagram of the local discharge demonstrates appreciable hysteresis loops compared with that of the local piling in Figure 4.10 (right corner). In the first local region (#1, from the bottom to 3d), the volume fraction is independent of the hopper angle and the orifice size at steady state as shown in Figure 4.22 (top), however the coordination number is dependent on the hopper angle, the orifice size, and the wall geometry. Thus, the phase transition has steady state scatter in the cluster of points as shown in Figure 4.22 (middle). The points have two distinct regimes: the steady state, like-liquid regime and the rapid like-gas state. The different geometries are correlated with the mass flow rate. The mass flow rate is shown in Figure 4.22 (bottom). The inner and outer of the mass flow rate are equal to the absolute value.

www.manaraa.com

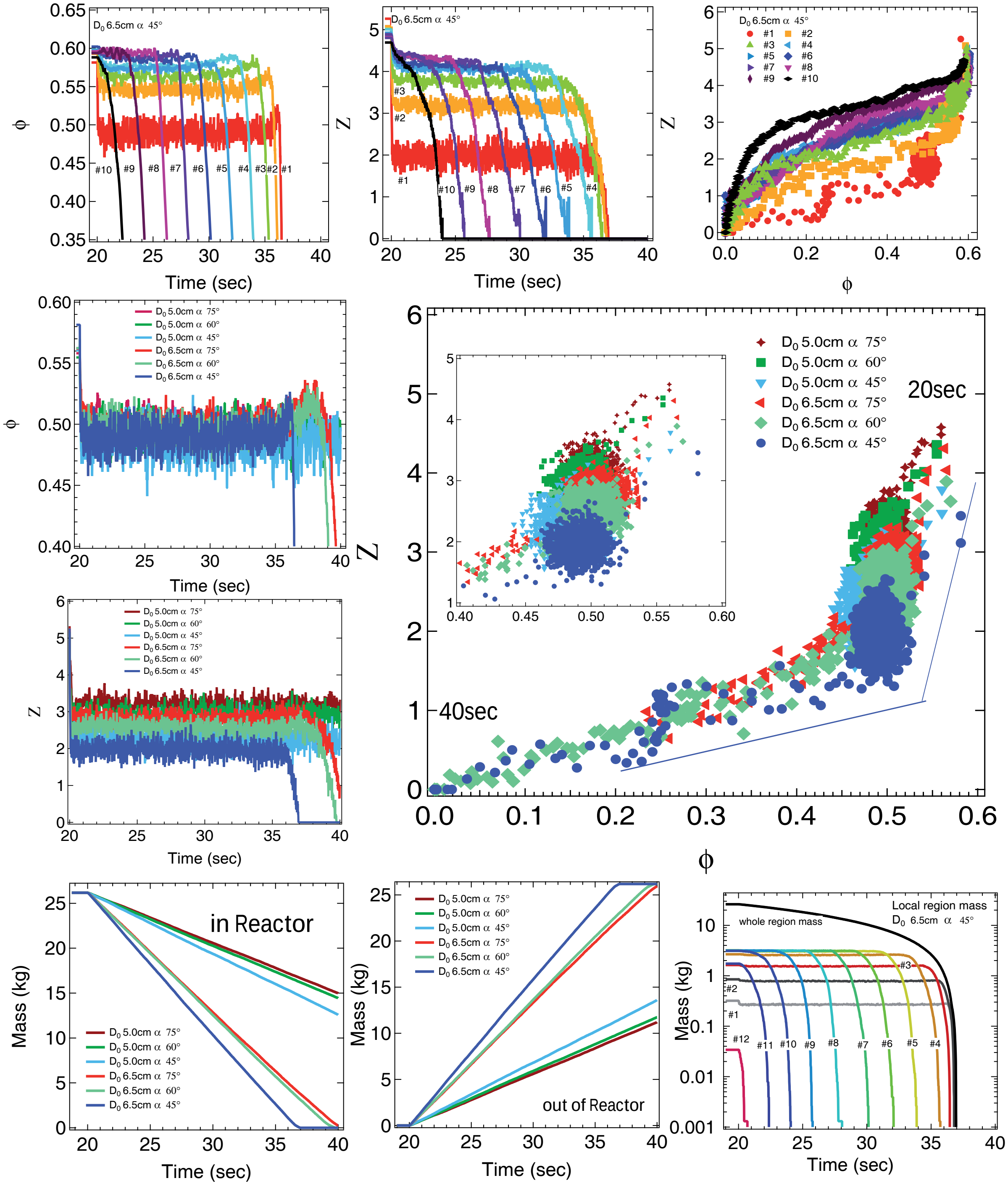

Figure 4.22: The different value of ϕ -z of each region (top), the phase diagram of ϕ -z on time evolution in first region between 0 and 3 cm (middle), the outlet and inner mass flow rate of whole system, and the inner local mass flow rate of each region (bottom)

www.manaraa.com

Chapter 5

Conclusions

5.1 Summary

The characteristics of the piling and the discharge in Pebble Bed Reactors (PBRs) were investigated with different types of hopper angles and orifice widths. Molecular Dynamics (MD) simulations were performed by regulating the orifice plate bottom to determine the effect of piling and discharge in PBRs. The process for MD simulations is divided into two types. One is piling and another is discharge. The discharge of the hopper can exhibit jamming or flowing. The mass flow rate of the piling and the discharge has been computed. The 3D imaging technique known as Paraview has been monitored to visualize the force, the translational velocity, and the angular velocity. The particle motion was also tracked throughout the simulations and lead to the analysis of the granular flow. The fundamental concepts in statistics mechanics were investigated, and a local phase diagram was developed and used to analyze the phase transition of the jamming and flowing condition. The gravitational potential and the kinetic energy were calculated to evaluate the granular temperature and compared with the results obtained from the force moment

المنارة للاستشارات
www.manaraa.com

tensor. The simulation results show that for 20,000 particles, the mass flow rate can be found to be correlated with the local phase transition of the discharge in the range of the local coordination number with the local volume fraction. Indeed, the geometry of the hopper is related to the orifice size and the hopper angle. The geometry conditions play a crucial role in the jamming and flowing, which are determined to use the wall stress and the phase diagram of the volume fraction and the coordination number on the real-time evolution. Particularly, the critical condition of the jamming is observed. The jamming geometry is in good agreement with the prototype Pebble Bed Reactor for radioisotope particle tracking in CEAR, Nuclear Engineering at North Carolina State University. The major advantages of the proposed system in MD simulations of LAMMPS/LIGGGHTS demonstrates comprehensively that the analysis of particle tracking in PBRs suggests further understanding of the experimental methods and designs.

5.2 Future Work

First of all, the velocity profile of the discharge will be compared with our New Kinematic Model. The model is associated with the volume fraction along the vertical and horizontal direction. For a continuum mechanics approach, the average wall stress obtained from the simulation results will be comparable to an analytical solution of the stress. For the scale up application, the mass flow rate is used to predict the optimal geometric condition to obtain an estimate of granular flows as follows the Beverloo equation. Finally, the energy functions of the piling and the discharge will be developed with the analytical solution, likely to be observed as a power law behavior.

المنارة للاستشارات
www.manaraa.com

REFERENCES

Aste, T. (2006). Volume fluctuations and geometrical constraints in granular packs. Physical Review Letters, Vol. 96, No. 1.

Aste, T., Saadatfar, M. & Senden, T.J. (2006). Local and global relations between the number of contacts and density in monodisperse sphere packs. Journal of Statistical Mechanics-Theory and Experiment.

Ball, R.C. & Blumenfeld, R. (2002). Stress field in granular systems: Loop forces and potential formulation. Physical Review Letters, Vol. 88, No. 11

Bernal, J.D. & Mason, J. (1960). Packing of Spheres: Co-Ordination of Randomly Packed Spheres. Nature, Vol. 188, No. 4754, pp. 910-911.

Beverloo, W.A., Leniger, H.A. & Vandevelde, J. (1961). The Flow of Granular Solids through Orifices. Chemical Engineering Science, Vol. 15, No. 3-4, pp. 260.

Brilliantov, N.V., Spahn, F., Hertzsch, J.M. & Poschel, T. (1996). Model for collisions in granular gases. Physical Review E, Vol. 53, No. 5, pp. 5382-5392.

Brown, R.L. & Hawksley, P.G.W. (1947). Modelling of Pressures and Flow in Silos. Fuel, Vol. 26, pp. 159-173.

Campbell, C.S. (1990). Rapid Granular Flows. Annual Review of Fluid Mechanics, Vol. 22, pp. 57-92.

Caram, H. & Hong, D.C. (1991). Random-Walk Approach to Granular Flows. Physical Review Letters, Vol. 67, No. 7, pp. 828-831.

Choi, J., Kudrolli, A. & Bazant, M.Z. (2005). Velocity profile of granular flows inside silos and hoppers. Journal of Physics-Condensed Matter, Vol. 17, No. 24, pp. S2533-S2548.

Choi, J., Kudrolli, A., Rosales, R.R. & Bazant, M.Z. (2004). Diffusion and mixing in gravity-driven dense granular flows. Physical Review Letters, Vol. 92, No. 17

Cundall, P.A. & Strack, O.D.L. (1979). Discrete Numerical-Model for Granular Assemblies. Geotechnique, Vol. 29, No. 1, pp. 47-65.

المنارة للاستشارات
www.manaraa.com

Edwards, S.F. & Oakeshott, R.B.S. (1989). Theory of Powders. Physica A, Vol. 157, No. 3, pp. 1080-1090.

Epstein, N. & Young, M.J. (1962). Random Loose Packing of Binary Mixtures of Spheres. Nature, Vol. 196, No. 4857, pp. 885.

Gan, Y.X., Kamlah, M. & Reimann, J. (2010). Computer simulation of packing structure in pebble beds. Fusion Engineering and Design, Vol. 85, No. 10-12, pp. 1782-1787.

Gardner, R.P., Barrett, C.L., Haq, W. & Peplow, D.E. (1996). Efficient Monte Carlo simulation of O-16 neutron activation and N-16 decay gamma-ray detection in a flowing fluid for on-line oxygen analysis or flow rate measurement. Nuclear Science and Engineering, Vol. 122, No. 3, pp. 326-343

Gougar, H.D., Ougouag, A.M. & Terry, W.K. (2004). Advanced core design and fuel management for pebble-bed reactors. Idaho National Engineering and Environmental Laboratory, Idaho Falls, Idaho 83415

Huang, K. (1987). Statistical mechanics, (2nd edn) New York: Wiley, p. xiv, 493 p. Jaeger, H.M., Nagel, S.R. & Behringer, R.P. (1996). Granular solids, liquids, and gases. Reviews of Modern Physics, Vol. 68, No. 4, pp. 1259-1273.

Johanson, J.R. (1965). Method of Calculating Rate of Discharge from Hoppers and Bins. Trans. Min. Engrs. AIME, Vol. 232.

Johnson, K.L. (1985). Contact mechanics. Cambridge; New York: Cambridge University Press. p. 1 online resource.

Kvapil, R. (1959). Theorie der Schttgutbewegung. VEB-Verlag Technik, Berlin. LAMMPS http://lammps.sandia.gov

Li, Y.J., Yong, X. & Jiang, S.Y. (2009). DEM simulations and experiments of pebble flow with monosized spheres. Powder Technology, Vol. 193, No. 3, pp. 312-318.

LIGGGHTS http://www.liggghts.com.

Makse, H.A., Johnson, D.L. & Schwartz, L.M. (2000). Packing of compressible granular materials. Physical Review Letters, Vol. 84, No. 18, pp. 4160-4163.

المنارة للاستشارات

www.manaraa.com

Mehta, A. & Barker, G.C. (1991). Vibrated Powders - a Microscopic Approach. Physical Review Letters, Vol. 67, No. 3, pp. 394-397.

Mehta, A. & Edwards, S.F. (1989). Statistical-Mechanics of Powder Mixtures. Physica A, Vol. 157, No. 3, pp. 1091-1100.

Mindlin, R.D. (1949). Compliance of Elastic Bodies in Contact. Journal of Applied Mechanics-Transactions of the Asme, Vol. 16, No. 3, pp. 259-268.

Nedderman, R.M. & Tuzun, U. (1979). Kinematic Model for the Flow of Granular-Materials. Powder Technology, Vol. 22, No. 2, pp. 243-253.

Nguyen, T., Brennen, C. & Sabersky, R.H. (1979). Gravity flow of granular materials in conical hoppers. J. Appl. Mech. ASME, Vol. 79-WA/APM-20.

Ono, I.K., O'Hern, C.S., Durian, D.J., Langer, S.A., Liu, A.J. & Nagel, S.R. (2002). Effective temperatures of a driven system near jamming. Physical Review Letters, Vol. 89, No. 9

Onoda, G.Y. & Liniger, E.G. (1990). Random Loose Packings of Uniform Spheres and the Dilatancy Onset. Physical Review Letters, Vol. 64, No. 22, pp. 2727-2730.

ParaView http://www.paraview.org.

Pugnaloni, L.A. & Barker, G.C. (2004). Structure and distribution of arches in shaken hard sphere deposits. Physica a-Statistical Mechanics and Its Applications, Vol. 337, No. 3-4, pp. 428-442.

Reif, F. (1965). Fundamentals of statistical and thermal physics, [by] F. Reif, New York,: McGraw Hill, p. x, 651

Rintoul, M.D. & Torquato, S. (1996). Metastability and crystallization in hard-sphere systems. Physical Review Letters, Vol. 77, No. 20, pp. 4198-4201.

Rycroft, C.H., Grest, G.S., Landry, J.W. & Bazant, M.Z. (2006). Analysis of granular flow in a pebble-bed nuclear reactor. Physical Review E, Vol. 74, No. 2

Scott, G.D. (1960). Packing of Equal Spheres. Nature, Vol. 188, No. 4754, pp. 908-909.

Silbert, L.E., Ertas, D., Grest, G.S., Halsey, T.C. & Levine, D. (2002). Geome-

المنارة للاستشارات
www.manaraa.com

try of frictionless and frictional sphere packings. Physical Review E, Vol. 65, No. 3

Silbert, L.E., Ertas, D., Grest, G.S., Halsey, T.C., Levine, D. & Plimpton, S.J. (2001). Granular flow down an inclined plane: Bagnold scaling and rheology. Physical Review E, Vol. 6405, No. 5

Song, C., Wang, P. & Makse, H.A. (2008). A phase diagram for jammed matter. Nature, Vol. 453, No. 7195, pp. 629-632.

Torquato, S. & Stillinger, F.H. (2010). Jammed hard-particle packings: From Kepler to Bernal and beyond (vol 82, pg 2633, 2010). Reviews of Modern Physics, Vol. 82, No. 4

Zhang, H.P. & Makse, H.A. (2005). Jamming transition in emulsions and granular materials. Physical Review E, Vol. 72, No. 1

المنارة للاستشارات
www.manaraa.com

APPENDICES

المنارة للاستشارات

www.manaraa.com

Appendix A

The phase diagram

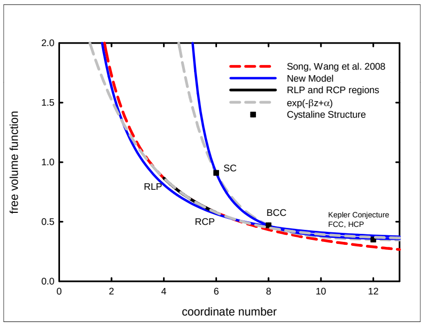

RLP (Random Loose Packing) $\phi_{RLP} \approx 0.55$

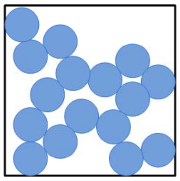

RCP (Random Close Packing, Bernal 1960) $\phi_{RCP} \approx 0.64$

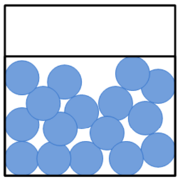

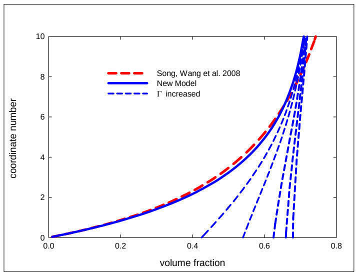

$$z = z_c + k \ln\left(1 - \Gamma + \frac{1}{1/\phi - 1/\phi_c}\right)$$

Crystalline structure

	CN	ϕ
simple cubic(sc)	6	0.52
body-centered cubic(bcc)	8	0.68
face-centered cubic(fcc)	12	0.74
hexagonal close-packed (hcp)	12	0.74

المنارة للاستشارات
www.manaraa.com

VOLUME 84, NUMBER 18 PHYSICAL REVIEW LETTERS 1 MAY 2000

Packing of Compressible Granular Materials

Hernán A. Makse, David L. Johnson, and Lawrence M. Schwartz
Schlumberger-Doll Research, Old Quarry Road, Ridgefield, Connecticut 06877

(Received 25 August 1999; revised manuscript received 22 December 1999)

3D computer simulations and experiments are employed to study random packings of compressible spherical grains under external confining stress. In the rigid ball limit, we find a continuous transition in which the stress vanishes as $(\phi - \phi_c)^\beta$, where ϕ is the (solid phase) volume density. The value of ϕ_c depends on whether the grains interact via only normal forces (giving rise to random close packings) or by a combination of normal and friction generated transverse forces (producing random loose packings). In both cases, near the transition, the system's response is controlled by localized force chains.

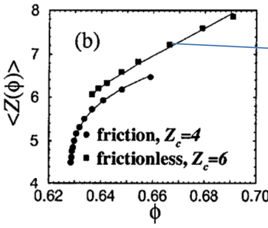

Vol 453|29 May 2008|doi:10.1038/nature06981 nature

LETTERS

A phase diagram for jammed matter

Chaoming Song[1], Ping Wang[1] & Hernán A. Makse[1,2]

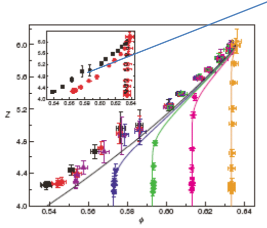

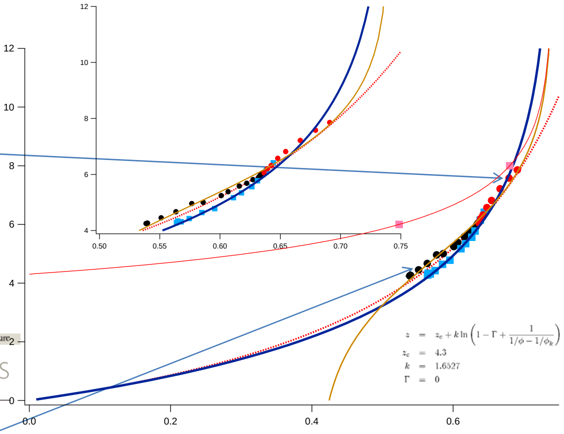

$$
\begin{aligned}
z &= z_c + k \ln\left(1 - \Gamma + \frac{1}{1/\phi - 1/\phi_k}\right) \\
z_c &= 4.3 \\
k &= 1.6527 \\
\Gamma &= 0
\end{aligned}
$$

$$z = 2\sqrt{3}\ln\left(1 + \frac{1}{1/\phi - 1/\phi_c}\right)$$

$$
\begin{aligned}
z &= z_c + k \ln\left(1 - \Gamma + \frac{1}{1/\phi - 1/\phi_c}\right) \\
z_c &= 4 \\
k &= 1.68
\end{aligned}
$$

VOLUME 84, NUMBER 18 PHYSICAL REVIEW LETTERS 1 MAY 2000

Packing of Compressible Granular Materials

Hernán A. Makse, David L. Johnson, and Lawrence M. Schwartz
Schlumberger-Doll Research, Old Quarry Road, Ridgefield, Connecticut 06877
(Received 25 August 1999; revised manuscript received 22 December 1999)

3D computer simulations and experiments are employed to study random packings of compressible spherical grains under external confining stress. In the rigid ball limit, we find a continuous transition in which the stress vanishes as $(\phi - \phi_c)^\beta$, where ϕ is the (solid phase) volume density. The value of ϕ_c depends on whether the grains interact via only normal forces (giving rise to random close packings) or by a combination of normal and friction generated transverse forces (producing random loose packings). In both cases, near the transition, the system's response is controlled by localized force chains.

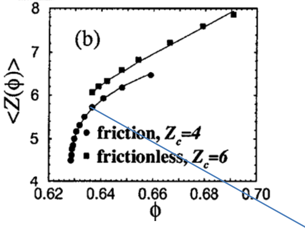

PHYSICAL REVIEW E 72, 011301 (2005)

Jamming transition in emulsions and granular materials

H. P. Zhang
Physics Department, City College of New York, New York 10031, USA

H. A. Makse
Physics Department and Levich Institute, City College of New York, New York 10031, USA

(Received 16 January 2005; published 7 July 2005)

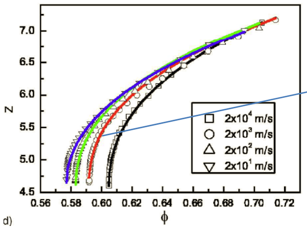

$\phi \approx 0.581 \pm 0.001$ and the mean coordination number $z = 6.00 \pm 0.02$ (Mehta and Barker 1991)

$$
\begin{aligned}
z &= z_c + k \ln\left(1 - \Gamma + \frac{1}{1/\phi - 1/\phi_c}\right) \\
z_c &= 6 \\
k &= 0.47
\end{aligned}
$$

Γ increased

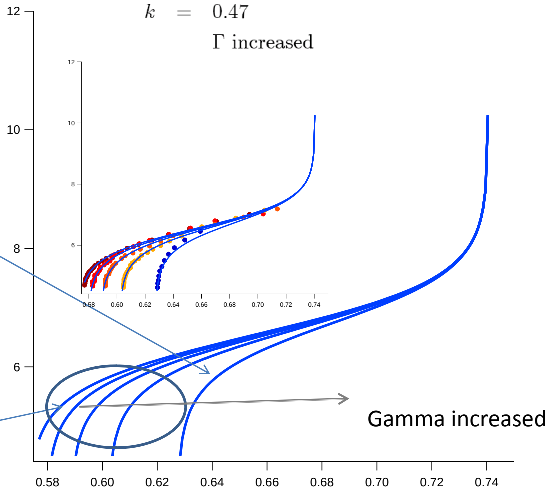

$$
\begin{aligned}
z &= z_c + h\,(\phi - \phi_c)^\beta \\
z_c &= 4
\end{aligned}
$$

www.manaraa.com

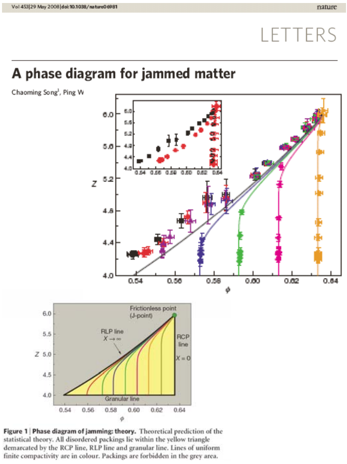
Vol 453|29 May 2008|doi:10.1038/nature06981 nature

LETTERS

A phase diagram for jammed matter

Chaoming Song[1], Ping W

Figure 1 | Phase diagram of jamming: theory. Theoretical prediction of the statistical theory. All disordered packings lie within the yellow triangle demarcated by the RCP line, RLP line and granular line. Lines of uniform finite compactivity are in colour. Packings are forbidden in the grey area.

$\phi \approx 0.55 \sim 0.61$ and the mean coordination number $z = 5.6 \pm 0.1$
Pugnaloni, L. A. and G. C. Barker (2004).

$$
\begin{aligned}
z &= z_c + k\ln\left(1-\Gamma+\frac{1}{1/\phi-1/\phi_c}\right)\\
z_c &= 5.5\\
k &= 0.47
\end{aligned}
$$

Γ increased

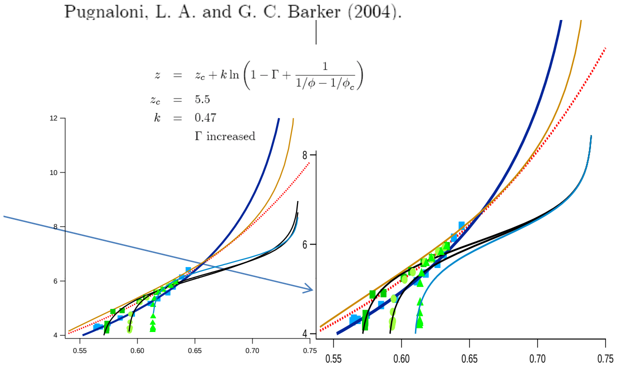

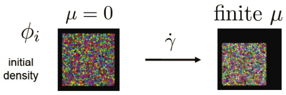

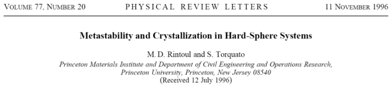
VOLUME 77, NUMBER 20 PHYSICAL REVIEW LETTERS 11 NOVEMBER 1996

Metastability and Crystallization in Hard-Sphere Systems

M. D. Rintoul and S. Torquato
Princeton Materials Institute and Department of Civil Engineering and Operations Research, Princeton University, Princeton, New Jersey 08540
(Received 12 July 1996)

$$
z = 5 + 0.28\ln\left(1-\Gamma+\frac{1}{\frac{1}{\phi}-\frac{1}{\phi_{RCP}}}\right)
$$

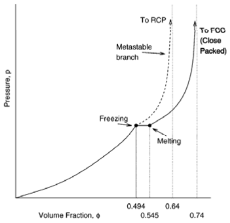

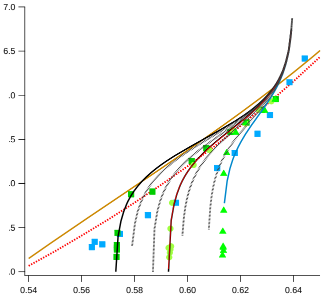

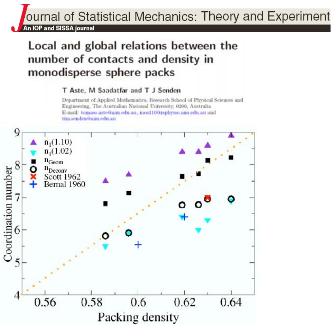
Journal of Statistical Mechanics: Theory and Experiment
An IOP and SISSA journal

Local and global relations between the number of contacts and density in monodisperse sphere packs

T Aste, M Saadatfar and T J Senden
Department of Applied Mathematics, Research School of Physical Sciences and Engineering, The Australian National University, 0200, Australia
E-mail: tomaso.aste@anu.edu.au, mos110@rsphysse.anu.edu.au and tim.senden@anu.edu.au

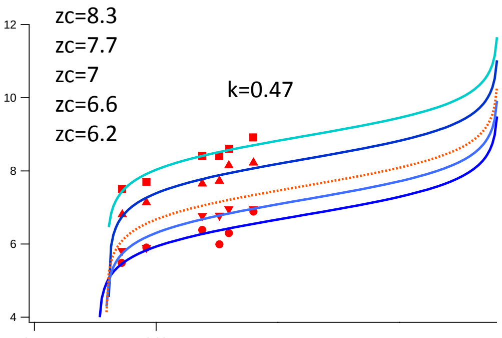

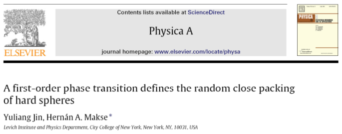
Contents lists available at ScienceDirect
Physica A
journal homepage: www.elsevier.com/locate/physa

A first-order phase transition defines the random close packing of hard spheres

Yuliang Jin, Hernán A. Makse*
Levich Institute and Physics Department, City College of New York, New York, NY, 10031, USA

$$
\begin{aligned}
z &= z_c + k\ln\left(1-\Gamma+\frac{1}{1/\phi-1/\phi_c}\right)\\
z_c &= 5.5\\
k &= 0.47
\end{aligned}
$$

Γ increased

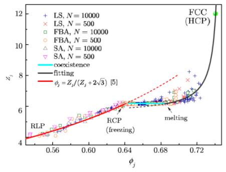

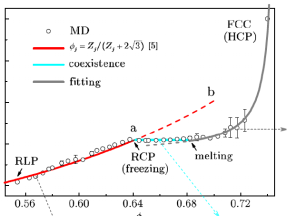

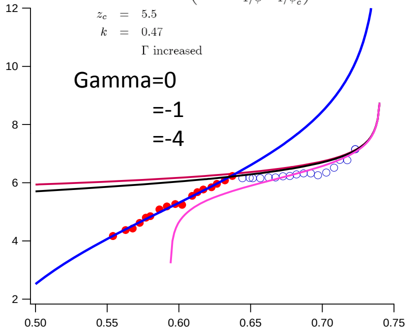

المنارة للاستشارات
www.manaraa.com

Appendix B

Volume calculations

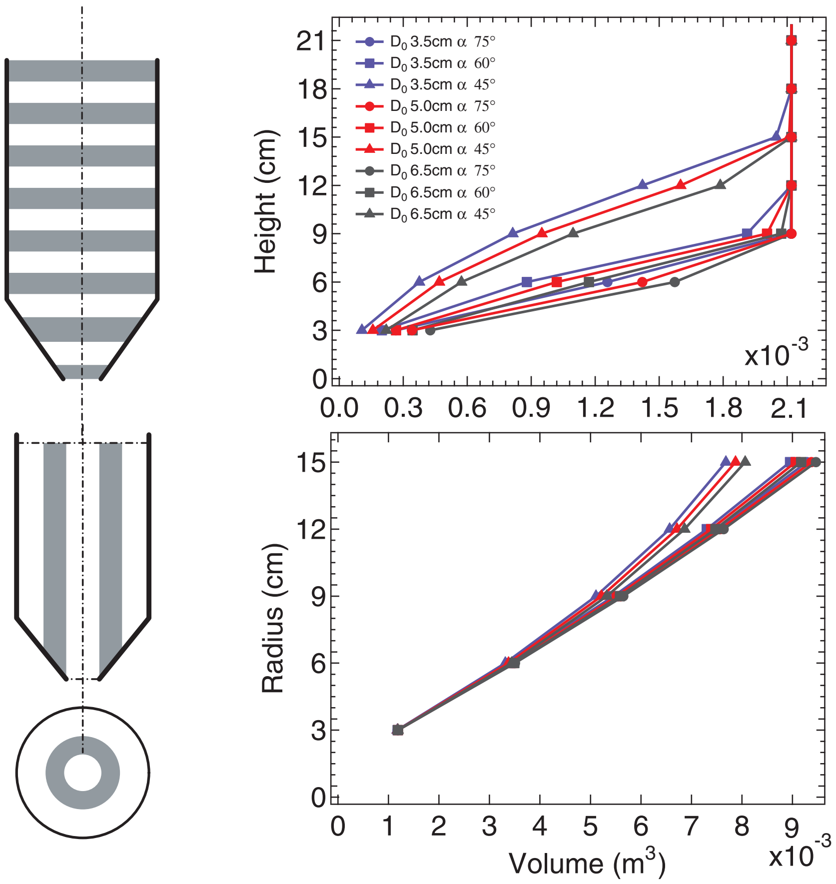

المنارة للاستشارات
www.manaraa.com

Appendix C

The stress in jamming

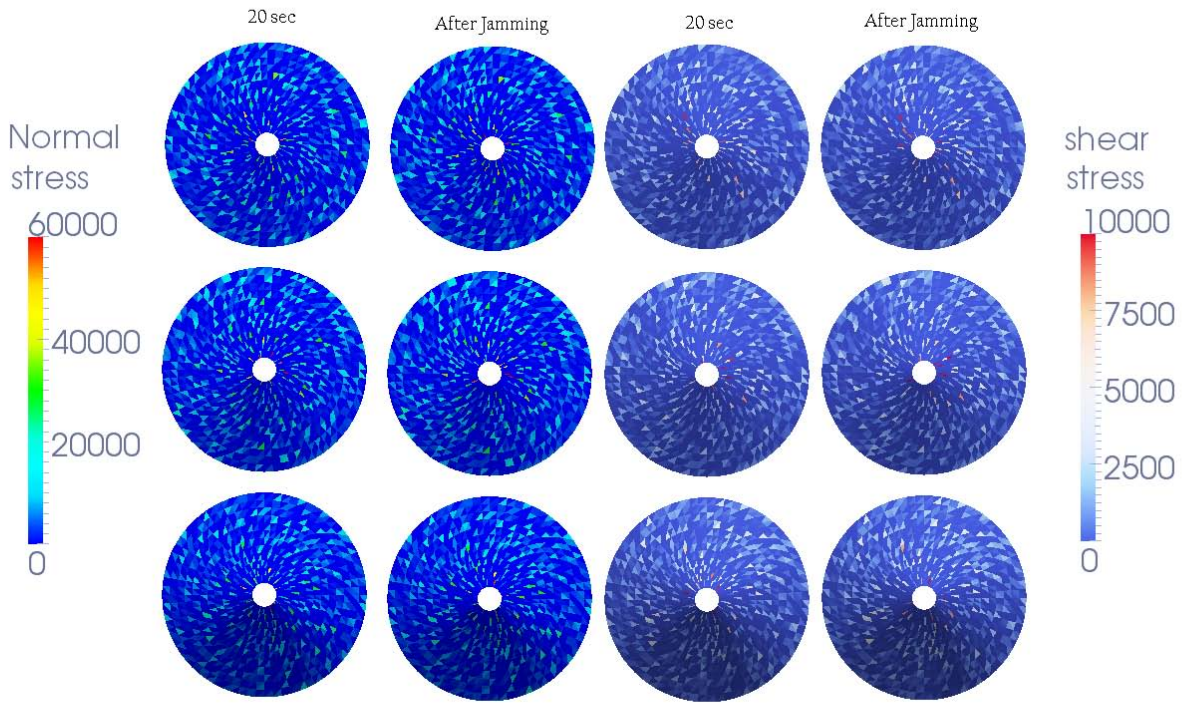

www.manaraa.com